CHALMERS
UNIVERSITY OF TECHNOLOGY

Photochemistry of a Photochromic Ruthenium Sulfoxide Complex for increased Understanding of Structure–Properties Relationship

Master's thesis in the Materials Chemistry programme

AUGUST GASSLANDER

Department of Chemistry and Chemical Engineering
CHALMERS UNIVERSITY OF TECHNOLOGY
Gothenburg, Sweden 2017

MASTER'S THESIS

Photochemistry of a Photochromic Ruthenium Sulfoxide Complex for increased Understanding of Structure–Properties Relationship

Department of Chemistry and Chemical Engineering
Division of Physical Chemistry
CHALMERS UNIVERSITY OF TECHNOLOGY
Göteborg, Sweden

Photochemistry of a Photochromic Ruthenium Sulfoxide Complex for increased Understanding of Structure–Properties Relationship
AUGUST GASSLANDER

Supervisor: Elin Sundin, Chalmers University of Technology
Examiner: Maria Abrahamsson, Chalmers University of Technology
Department of Chemistry and Chemical Engineering
Division of Chemistry and Biochemistry
Chalmers University of Technology
SE–412 96 Göteborg
Sweden
Telephone: + 46 (0)31–772 1000

Göteborg, Sweden

Photochemistry of a Photochromic Ruthenium Sulfoxide Complex for increased Understanding of Structure–Properties Relationship

Department of Chemistry and Chemical Engineering
Division of Physical Chemistry
Chalmers University of Technology

Abstract

Dye Sensitized Solar Cells and the similar Dye Sensitized Photoelectrosynthesis Cells are potential low cost alternatives to conventional solar technology, which utilize a dye to absorb sunlight. A group of potential dye candidates are the ruthenium sulfoxide complexes with their possibly beneficial S– to –O isomerization mechanism. In this project, the ruthenium sulfoxide complex $[Ru(deeb)_2PyMeSO–iPr]^{2+}$ (deeb is 4,4'–diethylester–2,2'–bipyridine, PyMe is 2–methylpyridine and iPr is isopropyl) is studied in the solvents CH_2Cl_2, propylene carbonate (PC) and acetonitrile (ACN) and on TiO_2 and ZrO_2 films, to characterize the photochemical and photophysical properties of the complex. Comparative experiments are done on the corresponding thioether $[Ru(deeb)_2PyMeS–iPr]^{2+}$ which lacks isomerization mechanism.

In this project, $[Ru(deeb)_2PyMeSO–iPr]^{2+}$ is found to demonstrate reversible S– to –O isomerization in non–coordinating solvents, and nearly complete photoinduced O– to –S reversion is possible with irradiation of 623 nm. In addition, O–bonded $[Ru(deeb)_2PyMeSO–iPr]^{2+}$ is demonstrated to spontaneously transition to S–bonded through thermal reversion. In the coordinating solvent ACN, both $[Ru(deeb)_2PyMeSO–iPr]^{2+}$ and thioether $[Ru(deeb)_2PyMeS–iPr]^{2+}$ form photoproducts in response to MLCT (Metal to Ligand Charge Transfer) irradiation. A possible explanation for this behavior is a photoinduced process where the ligands of the ruthenium complexes are replaced by ACN molecules.

S– to –O isomerization and photoinduced O– to –S reversion of $[Ru(deeb)_2PyMeSO–iPr]^{2+}$ anchored to TiO_2 and ZrO_2 films is also demonstrated, as well as thermal reversion on TiO_2. Rate constants for isomerization and reversion in different environments are estimated through the fitting of kinetic traces to mono– or biexponential models. O– to –S isomerization of $[Ru(deeb)_2PyMeSO–iPr]^{2+}$ is faster in PC than in CH_2Cl_2, indicating a kinetic stabilization of the O–bonded isomer in CH_2Cl_2 relative to PC. In addition, initial O– to –S reversion is faster on TiO_2 film immersed in CH_2Cl_2 than in CH_2Cl_2 solution, indicating that the O-bonded form is more kinetically stable in solution than on film.

Abbreviations

A	=	Electron acceptor
ACN	=	Acetonitrile
bpy	=	2,2'–Bipyridine
CB	=	Conduction band
deeb	=	4,4'–diethylester–2,2'–bipyridine
DMSO	=	Dimethylsulfoxide
DSPEC	=	Dye Sensitized Photoelectrosynthesis Cell
DSSC	=	Dye Sensitized Solar Cell
ES	=	Excited State
GS	=	Ground State
LMCT	=	Ligand to Metal Charge Transfer
MC	=	Metal Centered
MLCT	=	Metal to Ligand Charge Transfer
P	=	Photosensitizer
PC	=	Propylene carbonate
TiO_2	=	Titanium(IV) oxide
VB	=	Valence band
ZrO_2	=	Zirconium(IV) oxide

Contents

1. Introduction

1.1 Background

Today, 97 % of the actively publishing climate scientists are convinced by the evidence showing that human pollution is the cause of climate change [1]. To stop global warming, the world therefore must move away from burning fossil fuels and instead use alternative energy sources. One way of doing this is to harvest the energy in sunlight, either for electricity generation or renewable fuel synthesis. Dye Sensitized Solar Cells (DSSC) or Dye Sensitized Photoelectrosynthesis Cell (DSPEC) are two types of devices which absorb sunlight and makes use of its energy [2][3].

DSSC:s and DSPEC:s work similarly. In both devices a dye is attached to a nanostructured semiconductor thin film, which gives enhanced absorption of sunlight. With the absorbed energy from the sun, electrons are injected from excited dye molecules into the conduction band of the semiconductor. From here the electrons can be used as electricity in DSSC:s or to drive reactions in DSPEC:s [2][3].

A lot of research has been done to optimize the different components used in dye sensitized semiconductor devices, including the dye molecule. The use of ruthenium polypyridine complexes as dyes has given some of the best results, as these complexes generally have strong absorption in the visible region, suitable excited state energies and redox levels, relatively long excited–state lifetime, and chemical stability [4]. Additionally the photophysical properties in ruthenium polypyridine complexes can be fine–tuned by ligand substitution [5]–[8].

The interest in ruthenium sulfoxide complexes, the focus of this work, begun in 1982 when Henry Taube and coworkers published their work on $[Ru(NH_3)_5(dmso)]^{2+}$ (dmso is dimethylsulfoxide)[9]. Taube's experiments showed that electrochemical oxidation of $[Ru(NH_3)_5(dmso)]^{2+}$ induced isomerization – the bond between ruthenium and dmso changed from S–bonded to O–bonded. Consecutive reduction resulted in a reversion to S–bonded dmso ligand. Importantly, the isomers showed a difference in $E^{\circ\prime}$. The potential for the S–bonded form was found to be 1.0 V vs. NHE compared to 0.1 V vs. NHE for the O–bonded, indicating that the O–bonded isomer stabilizes the oxidized Ru(III) state [9]. A kinetically stable oxidized state is potentially associated with a slower rate of recombination, and is therefore a desired property for dye molecules used in DSSC:s [4].

The combination of ruthenium sulfoxide chemistry with ruthenium polypyridyl chemistry was pioneered 1987 when Roeker and Meyer showed that adding Me_2S to $[Ru(bpy)_2(py)(O)]^{2+}$ (bpy

is 2,2'–bipyridine, py is pyridine) produced an O–bonded $[Ru(bpy)_2(py)(dmso)]^{2+}$ complex, which spontaneously isomerized to the S–bonded form [10]. In theory, the combination of suitable dye properties of polypyridyl ligands with a stabilizing mechanism of Ru(III) could make an efficient dye.

In this project $[Ru(deeb)_2PyMeSO–iPr]^{2+}$ (where deeb is 4,4'–diethylester–2,2'–bipyridine, PyMe is 2–methylpyridine and iPr is isopropyl) is characterized. $[Ru(deeb)_2PyMeSO–iPr]^{2+}$ has both polypyridyl and sulfoxide ligands and is an analog to the previously studied $[Ru(bpy)_2PyMeSO–iPr]^{2+}$ [11]. Deeb ligands make it possible to anchor the complex to films, and should increase absorption in the visible spectrum by a red–shift of the MLCT (Metal to Ligand Charge Transfer) peaks compared to with bpy ligands. The red–shift due to deeb ligands can be seen clearly in the comparison between $[Ru(bpy)_3]^{2+}$ displaying a 455 nm MLCT peak, compared to $[Ru(deeb)_3]^{2+}$ with a 465 nm MLCT peak [12], [13]. Thus $[Ru(deeb)_2PyMeSO–iPr]^{2+}$ is an interesting complex to study for increased understanding of the relationship between chemical structure and properties in ruthenium sulfoxide complexes. $[Ru(deeb)_2PyMeSO–iPr]^{2+}$ can be seen in figure 1A.

For comparison, the corresponding thioether $[Ru(deeb)_2PyMeS–iPr]^{2+}$ in figure 1B is studied. This complex provides no sulfoxide group and consequently lacks the isomerization mechanism. Comparison of photophyscial and photochemical properties between the two complexes gives mechanistic insight.

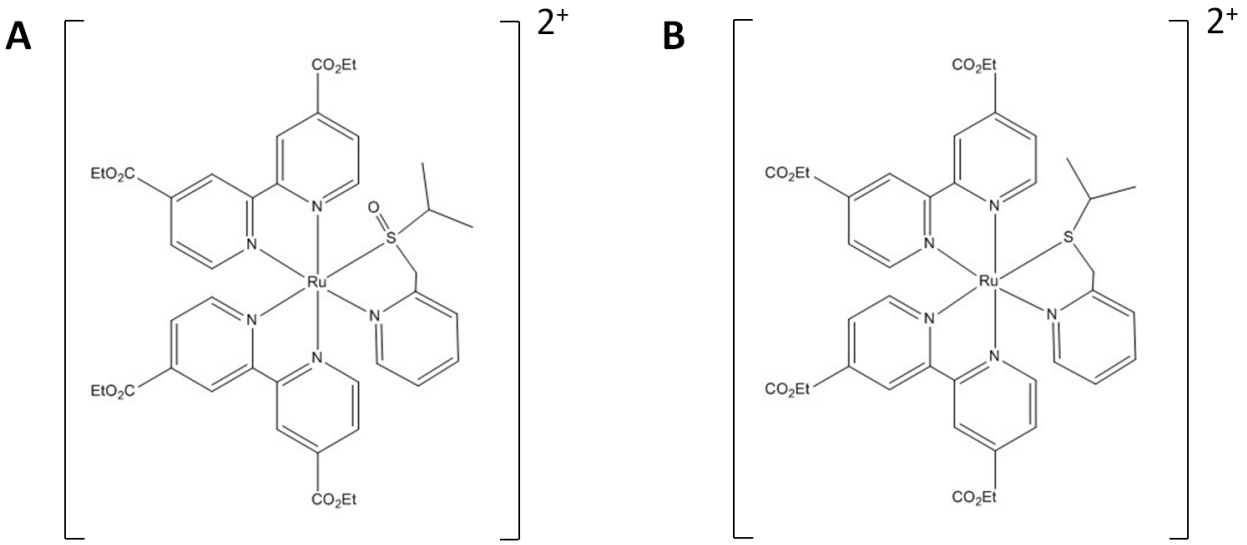

Figure 1: *Structures of the complexes studied in this project.* ***A)*** *$[Ru(deeb)_2PyMeSO–iPr]^{2+}$ and* ***B)*** *corresponding thioether $[Ru(deeb)_2PyMeS–iPr]^{2+}$.*

1.2 Purpose of project

The purpose of the project is photophysical and photochemical characterization of the ruthenium complex $[Ru(deeb)_2PyMeSO–iPr]^{2+}$ and the reference complex $[Ru(deeb)_2PyMeS–iPr]^{2+}$. The photochemistry of the compounds was investigated in coordinating and non–coordinating solvents and when anchored to mesoporous nanocrystalline semiconductor thin films.

Characterization of $[Ru(deeb)_2PyMeSO–iPr]^{2+}$ and $[Ru(deeb)_2PyMeSO–iPr]^{2+}$ expands the knowledge of ruthenium sulfoxide complexes, and gives insight into the relationship between structure and properties in ruthenium complexes in general. The understanding of surface–dye interaction of ruthenium sulfoxide complexes is also increased. The characterization is thus important for many scientific fields, such as the design of future dyes.

2. Theory

2.1 Quantized energy levels in matter

In the macroscopic world, classical physics accurately describe particles and their properties such as energy and position. Classical particles are assumed to be able to have any energy. While this approximation works fine in the macroscopic world, atomic scale systems show behavior which does not agree with these predictions. Instead, it is evident that particles confined in small volumes (such as an electron in a hydrogen atom) have only a discrete number of allowed energy levels. To understand why small systems have discrete energy levels, quantum mechanics and the wave–particle duality of matter must be considered [14].

The famous Schrödinger equation is a means of describing the quantum mechanical behavior of particles confined in space, such as an electron in an atom. When solving the Schrödinger equation it yields a set of possible *wave functions*. The wave function describes the behavior of the particle or wave and gives the possible positions of where it can be found. From the wave function it is possible to construct *atomic orbitals* which represent a volume where the electron has high probability of being found. As there is a set of wave functions generated by the Schrödinger equation, there is also a set of atomic orbitals. These orbitals differ in shape and relative energy.[14]

In a molecule, *molecular orbitals* are typically constructed from linear combinations of the atomic orbitals. The combination yields orbitals with new energy levels.[14] In figure 2 the molecular orbitals in H_2 are illustrated, represented by their energy level.

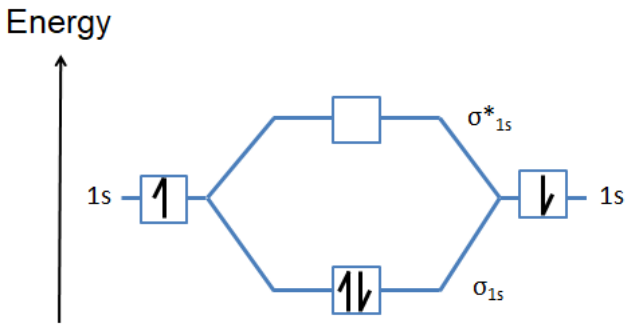

Figure 2: *Illustration of the energy levels of the orbitals in a hydrogen molecule, with HOMO σ_{1s} and LUMO σ^*_{1s}.*

According to the Aufbau principle, electrons will occupy the lowest energy orbitals that are available. Additionally the Pauli Exclusion Principle states that two electrons can only be in the

same orbital if they have antiparallel spin, also referred to as being paired. The *highest occupied molecular orbital* (HOMO) is the highest energy orbital that is occupied in a molecule in its ground state. The *lowest occupied molecular orbital* (LUMO) is the lowest energy orbital that is unoccupied in the ground state. When an electron is promoted from an occupied to an unoccupied orbital, the molecule is said to be excited [14]. Furthermore, the molecule can be in different states depending on if all electrons are paired, or if there are two unpaired electrons. The paired state is referred to as a singlet state, often denoted S_n, while an unpaired state is called a triplet state which is denoted T_n [15]. A triplet excited state T_n always has a lower energy than the corresponding singlet excited state [16].

In addition to the energy levels of orbitals there are also vibrational and rotational energy levels. Electronic energy levels together with vibrational energy levels are important when matter interacts with visible light [15]. This interaction is important in solar energy applications, as the visible region is the highest intensity part of solar radiation [17]. Thus it is desired to efficiently harvest the energy in this region.

2.2 Light–matter interactions

To explain light and its interactions the wave–particle duality of photons has to be considered. A photon cannot be described solely as particle or solely as a wave, as experiments has proven that the photon can behave as both a wave and a particle. The photoelectric effect strongly supports photons behaving like particles, while phenomena such as diffraction indicate that light behaves like waves [14].

Light can be described as an oscillating magnetic field and an oscillating electric field that propagates in a direction through space. This oscillating electromagnetic field can perturb molecules and induce transitions from one state to another [18]. Different wavelengths of light correspond to different energies through the relationship

$$E = hc/\lambda \qquad \text{(Eq. 1)}$$

where h is planck's constant, c speed of light and λ the wavelength of the radiation. If the energy of a photon equals the energy required for an electronic or vibronic transition, that photon can be absorbed [14].

A Jablonski diagram is often used to illustrate the energies of electronic states in a molecule, the possible transitions between these states and by which mechanisms these transitions can occur [19]. Such a diagram is depicted in figure 3.

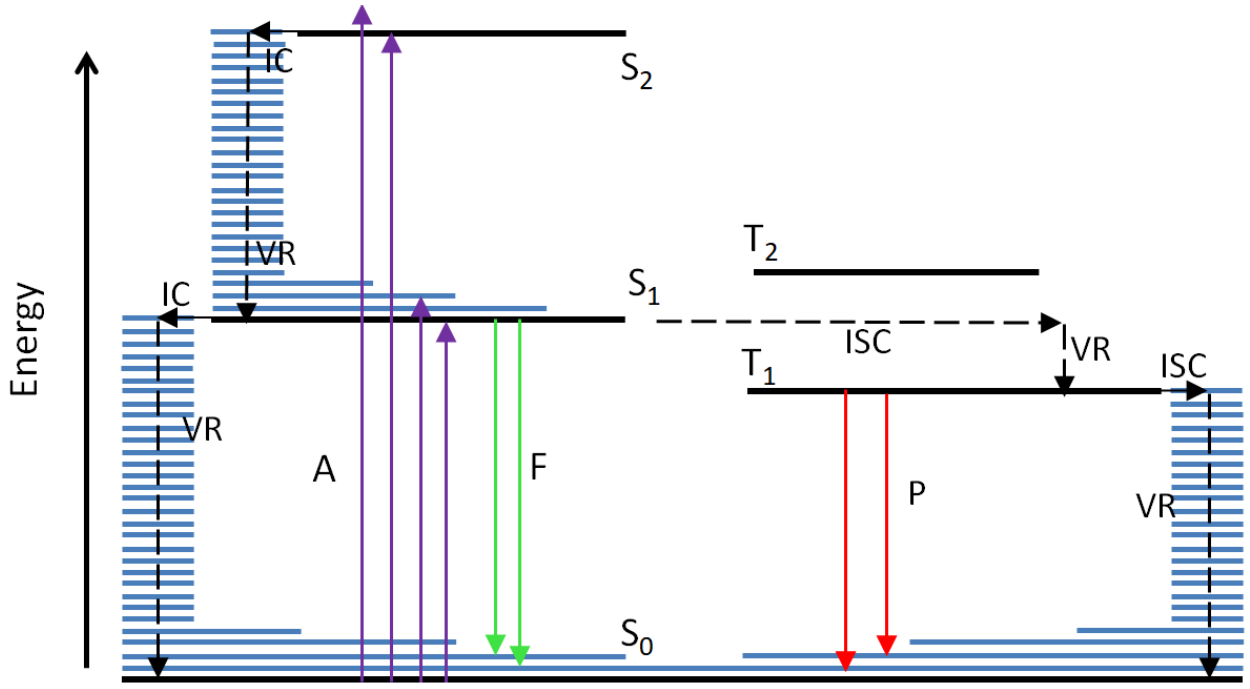

Figure 3*: A Jablonski diagram showing the electronic and vibrational energy levels and transitions between them.*

From its ground state (S_0), a molecule can be excited to a higher energy state through *absorption* of a photon, provided the energy of the photon equals an energy gap. Following this excitation, the molecule relaxes to singlet state S_1 through internal conversion (IC) and vibrational relaxation (VR) releasing energy as heat. S_1 can transition to ground state through fluorescence emitting a photon, or non–radiatively through IC and vibrational relaxation. S_1 can also undergo intersystem crossing (ISC) to populate the T_1 state. The emission of a photon when T_1 transitions to S_0 is called phosphorescence (P) [19]. The rates of these relaxation pathways differ significantly; generally k_{VR}, k_{IC} are approximately 10^{12} s^{-1} while ISC is spin–forbidden and generally slower. However, in heavy atom systems with strong spin–orbit coupling such as ruthenium complexes, the k_{ISC} rate constant can be around 10^{12} s^{-1}. k_F is typically near 10^8 s^{-1}, while k_P is typically several orders of magnitude slower. Phosphorescence is slower because of the forbiddance of a triplet to singlet transition [19].

2.3 Dye sensitized solar cells and dye sensitized photoelectrosynthesis cells

One example of a possible application of $[Ru(deeb)_2PyMeSO–iPr]^{2+}$ is as a dye in Dye Sensitized Solar Cells (DSSC) or in Dye Sensitized Photoelectrosynthesis Cell (DSPEC).

The backbone of DSSC:s and DSPEC:s is the semiconductor, and one of the most used semiconductors is TiO_2. In a semiconductor at room temperature, the electrons in the HOMO are referred to as resting in the *valence band* (VB). The electrons in VB do not have sufficient energy to be mobile, making the semiconductor non–conductive. However, with the input of energy, electrons can be promoted to the *conduction band* (CB) where the mobility of the electrons is increased. With electrons in CB the semiconductor becomes conductive, enabling transport of these electrons for electricity generation or reactions. The energy needed to promote an electron from VB to CB corresponds to the *band gap*. The semiconductor can absorb light of wavelengths corresponding to the band gap, leading to population of the CB [4].

A problem with TiO_2 in solar energy devices, is that they do not absorb visible light [4]. The visible spectrum is the highest intensity region of solar radiation reaching the earth and thus important to harvest [17]. A solution is to sensitize the semiconductor to the visible spectrum by adsorption of a light absorbing dye on the semiconductor. The high energy dye electrons generated by visible light absorption can be injected into the semiconductor CB, if the energy level of the dye excited state is higher than the lower edge of the conduction band. Injected electrons can then be used as electricity or for chemistry [3][4]. As electrons in the TiO_2 film is within a few nanometers distance from the dye, back electron transfer from the CB to the oxidized dye can occur. The back electron transfer should be minimized to avoid losing electrons which could be used for electricity generation or reactions [4]. A schematic representation of the bands, dye energy levels, injection and backward electron transfer can be seen in figure 4.

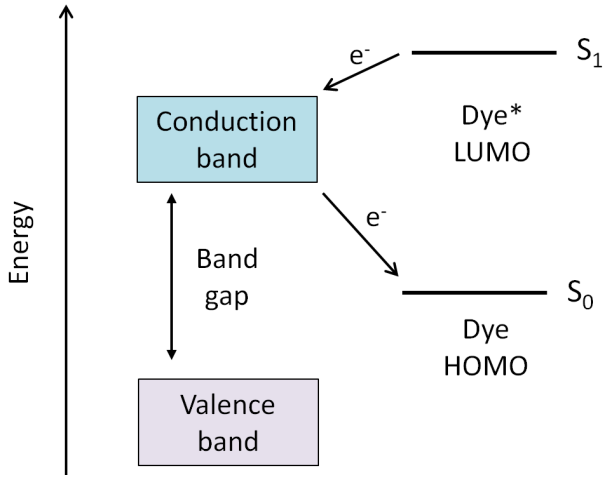

Figure 4: *Illustration of valence band, conduction band, band gap in the semiconductor TiO_2 and energy levels of dye. Electron injection can occur if the energy level of the dye excited state is higher than the lower edge of the conduction band. Additionally backward electron transfer from TiO_2 to dye is possible. The figure is adapted from* [20].

In a DSPEC device, the aim is to transport injected dye electrons via the semiconductor CB to a catalyst where electrons then can be used to catalyze reduction reactions [20]. One example of a desirable reaction is the reduction of carbon dioxide (CO_2) to methane (CH_4). However, photoinduced CO_2 to CH_4 reduction has to the best of my knowledge not yet been achieved with visible light. Figure 5 shows a schematic illustration of a DSPEC and its theoretical working principle.

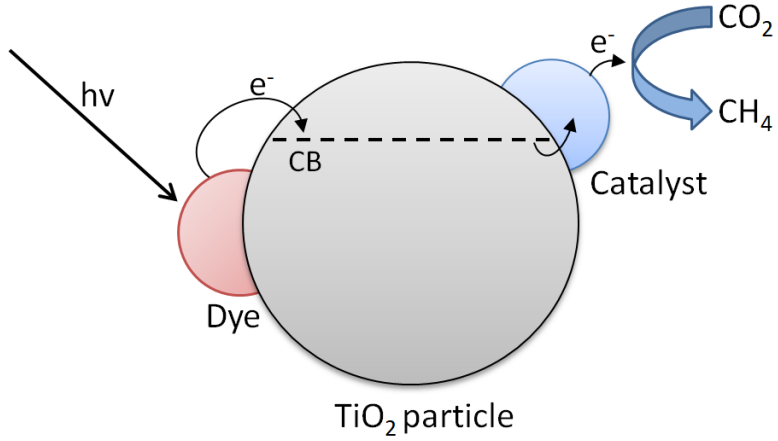

Figure 5: *Schematic illustration of a DSPEC and its working principle. Dye electrons are transferred to a reducing catalyst via the TiO_2 conduction band. The figure is adapted from* [20].

Desirable properties of a photosensitizer is strong and wide absorption in the visible spectrum, an excited energy level which is higher than the energy level of the semiconductor CB , long excited–state lifetime, and chemical stability in the oxidized state. The rate of injection also

must be faster than the rate of relaxation in dye to prevent excited state decay instead of electron injection [4].

2.4 Ru(II)–polypyridyl complexes

Many Ru(II)–polypyridyl complexes have been successfully used as dyes in DSSC:s and DSPEC:s, as these molecules generally have desirable properties for the application. Such properties are strong absorption in the visible region, suitable distribution of energy levels, and chemical and electrochemical stability [4]. Additionally, polypyridyl ligands can be substituted in order to tune properties such as the energy level distribution [5]–[8]. These traits have led to a lot of research being made on ruthenium polypyridyl complexes [21]–[29].

The energy levels in a photosensitizer are important. The excited state (ES) of the dye should be higher in energy than the semiconductor CB, and relative placement of other energy levels determines the excitation energies and thereby absorption spectrum. In addition, the excited state energy level and the redox potential of the photosensitizer and the electron acceptor affect the driving force for electron injection, as expressed in equation 2, defined by Rehm and Weller [30].

$$\Delta G° = (E_{1/2}(P^{ox/red}) - E_{1/2}(A^{ox/red}) - E°° + w \qquad \text{(Eq. 2)}$$

Where $E_{1/2}$ is the reduction potential for the photosensitizer and the acceptor, $E°°$ is the excited state energy of the lowest excited state ,and w summarizes the coulombic interaction [30]. A strong driving force is desired for efficient electron injection. Relative placement of the energy levels also affect the spontaneous decay pathways employed, which impacts the excited state lifetime as different decay processes vary in rate. A long excited state lifetime is desired to allow the excited dye to inject electrons before it relaxes to ground state (GS) [4], [5].

When discussing energy levels in transition metal complexes, including ruthenium complexes, it is appropriate to begin with some general transition metal complex theory. Upon ligand coordination the energy levels of the five d–orbitals in ruthenium split from degenerate to having different values. Three low energy t_{2g} orbitals and two high–energy e_g orbitals are formed. The spacing between these levels, Δ_O, is referred to as the *ligand field splitting parameter*. The ligand field splitting parameter is dependent on the coordinating ligands [14]. Ligand field splitting in ruthenium complexes is important for example since it gives rise to d→d transitions which is what generally gives transition metal complexes their strong color [18]. Ligand field splitting is schematically illustrated in figure 6.

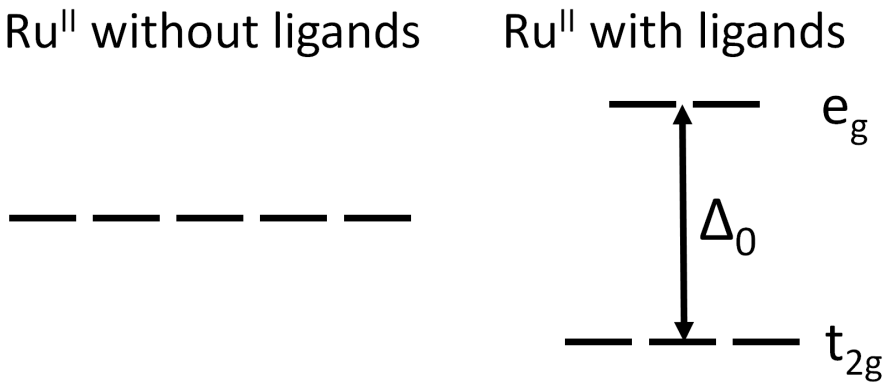

Figure 6: *Ligand coordination splits the five degenerate d–orbitals into three low energy t_{2g}–orbitals and two high energy e_g–orbitals.*

Apart from d→d transitions, another type of excitation in metal complexes are *metal to ligand charge transfer* (MLCT), in which an electron is promoted from a mainly metal localized orbital to a mainly ligand localized orbital. One example of MLCT is the promotion of an electron from a d–orbital (mainly metal localized orbital) to π*(mainly ligand localized orbital) [31]. In complexes with low lying π*–orbitals the MLCT transition can become the HOMO → LUMO transition. This is the case for some Ru(II)–polypyridyl complexes, for example $[Ru(bpy)_3]^{2+}$ [5]. The energy levels of Ru(II)–polypyridyl complexes are illustrated schematically in figure 7. In $[Ru(bpy)_3]^{2+}$ the MLCT excitation lies in the visible spectrum at 455 nm [12]. MLCT transitions usually have high extinction coefficients since they involve large *transition dipole moment* – a change in dipole of the molecule owing to the transition. High extinction coefficients are desired in solar energy harvesting applications [32].

It is possible to modify the MLCT state energy by changing the π^*_L energy level. For $[Ru(bpy)_3]^{2+}$, this can be done by substitution with electron withdrawing or electron donating groups on the bpy ligands. Electron withdrawing groups will increase the electron affinity of the ligand, which can stabilize a state with a formally reduced ligand such as the MLCT excited state [5]–[8]. This stabilization can result in longer excited state lifetimes [33], and might be observed spectroscopically as a red shift of the MLCT peak [5]. If bpy ligands are instead substituted with electron donating groups, this can result in a higher energy MLCT excited state and a blue shift of the MLCT peak [5]–[8].

For a long excited state lifetime fast pathways from the ES to GS should be avoided. For this to happen, states involved in rapid excited state decay should have much higher energy level than the excited state, and therefore have low probability of being accessed [18].

In figure 7 important deexcitation pathways are shown. Following MLCT excitation, the π^*_L state (or ^{1}MLCT) quickly and with a quantum yield close to unity fall down to ^{3}MLCT by ISC. The

^{3}MLCT state can transition, non–radiatively or radiatively to GS, or get thermally activated and populate ^{3}MC (indicated with red). The ^{3}MC state decays back to GS through fast non–radiative decay [5]. Population of ^{3}MC state can also result in cleavage of Ru–N bonds leading to ligand substitution in coordinating solvents [34]. For these reasons population of ^{3}MC is unfavorable for photosensitizers.

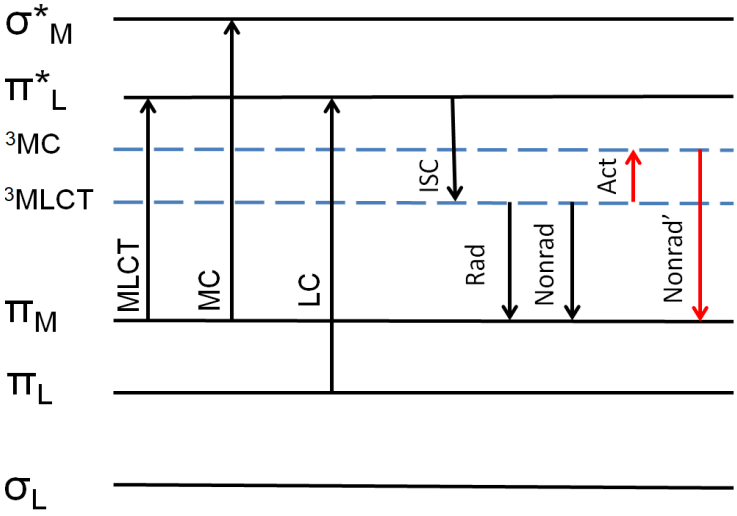

Figure 7: *Schematic illustration of transitions between states and orbitals in Ru-polypyridyl complexes, such as absorption processes and transitions from π*$_L$ to ground state. Note that the ^{3}MC state can vary in spacing and ordering relative to the ^{3}MLCT state. Figure adapted and modified from [35].*

As ΔO affects the energy levels of t_{2g} and e_g orbitals, Δ_O also affects the ^{3}MC energy level. A large Δ_O increases the energy level of ^{3}MC and therefore results in long excited state lifetime and a chemically stable complex [14], [36]. The magnitude of Δ_O together with the magnitude of the ES–GS energy gap (by the energy gap law) are the most important factors for a long lived excited state [5].

3. Method and materials

3.1 Chemicals

- Dimethyl sulfoxide (DMSO) (≥99.9% Sigma–Aldrich)
- Acetonitrile (MeCN) (≥99.5% Sigma–Aldrich)
- Ethanol (99,7%, Solveco)
- Methanol (MeOH) (99.6% Sigma–Aldrich)
- Titanium dioxide paste (18NR–T, Dyesol)
- ZrO_2 paste –Synthesized prior to project
- Acetone (99.98%, Fisher Scientific)
- Dichloromethane (99.8% Sigma Aldrich)
- Propylene Carbonate (PC) (anhydrous, 99,7%)
- RBS™ 25 solution (Concentrate Sigma Aldrich)
- $[Ru(deeb)_2PyMeSO–iPr]PF_6$ (synthesized by Fredrik Johansson, PhD student at Chemistry and Chemical Engineering department, Chalmers University of Technology)
- $[Ru(deeb)_2PyMeS–iPr]PF_6$ (synthesized by Fredrik Johansson, PhD student at Chemistry and Chemical Engineering department, Chalmers University of Technology)

3.2 Equipment

- Cuvette QS High Precision Cell Hellma Analytics 10 x 10 mm
- Spectrophotometer Varian Cary 50 Bio UV–Vis
- Emission spectrophotometer Horiba Fluorolog 3 FL3–22
- Power supply Manson EP–613
- LED lamps LED Engin Inc.
    - LZ1–00UB00 (385–410 nm)
    - LZ1–00B200 (460 nm)
    - LZ1–00G100 (523 nm)
    - LZ1–00R100 (623 nm)
- Power meter OPHIR Starlite Meter Assy Rohs
- Large Glass slides (127 x 102mm) TED PELLA, INC.
- Sintering oven ENTECH ETF 40/12

3.3 Steady state absorption spectroscopy

In Steady State Absorption Spectroscopy light is passed through a sample and the intensities before (I_0) and after passing through the sample (I) are compared [14]. In this project a Varian Cary 50 Bio UV–Vis spectrophotometer was used for the measurements. Absorption measurements can be used to determine the molar absorption coefficient through Lambert–Beer's law (Eq. 3).

$$A = -\log (I_o/I) = \varepsilon c l \qquad \text{(Eq. 3)}$$

Where *A* is absorbance, *ε* the molar absorption coefficient, *c* the concentration, and *l* path length of light through the sample [14]. In figure 8 the experimental setup of steady state absorption is illustrated.

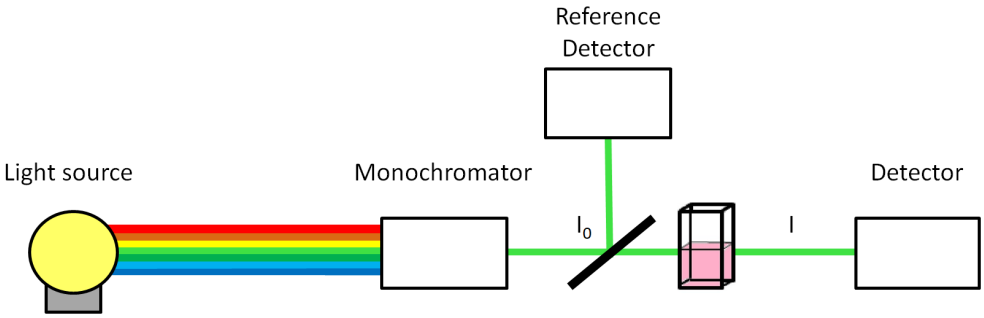

Figure 8: *Schematic illustration of experimental setup used for steady state absorption.*

3.4 Photolysis experiments

Photolysis experiments have been carried out by irradiating the sample with continuous light while simultaneously recording the absorption spectra of the sample. Thus the light induced chemical changes in molecules can be monitored. The photolysis experimental setup is identical to figure 8, with the addition of an exciting light source placed so that it hits the sample perpendicular to the probe light. In this project the exciting light source has been different monochromatic 385, 460, 523 and 623 nm LZI LED lamps (see section 3.1 for details). The power of the LED light on the sample has been constant, 0.9–1.0 mW. The experiments were carried out in a dark room under an IR lamp.

3.5 Steady state emission spectroscopy

The setup used for emission measurements is illustrated in figure 12. When collecting the excitation spectra, the monochromator scans an interval of excitation wavelengths and the emission at a specific wavelength is recorded. When collecting the emission spectra, the monochromator 1 selects one excitation wavelength and the full emission spectrum is recorded for this excitation. The beam is split to a reference detector to monitor the intensity of the excitation light during the measurement to correct for variations in the excitation light.

In figure 9 the experimental setup used for steady state emission spectroscopy is illustrated.

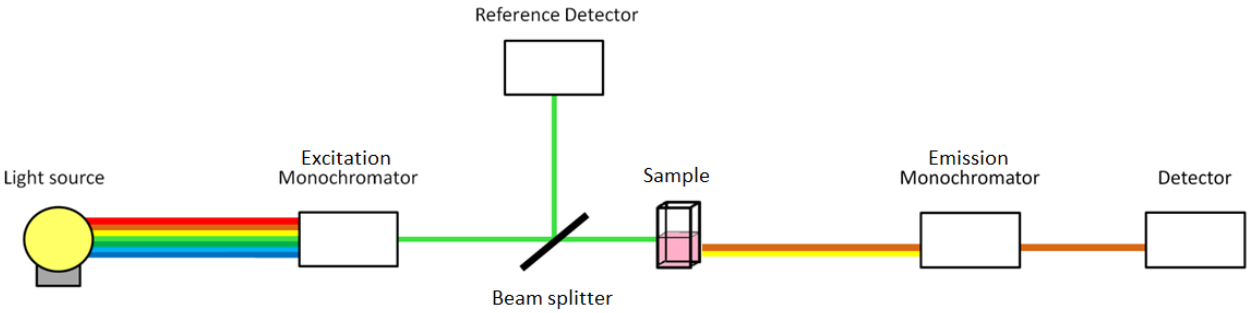

Figure 9: *Experimental setup of emission spectrophotometer used in project.*

3.6 Nanocrystalline mesoporous thin films of TiO_2 and ZrO_2

3.6.1 Preparation of glass slide

A diamond tip was used to cut glass slides which were put in an ultrasonic bath for 15 minutes in 2% RBS solution in MQ water. The slides were then rinsed with ethanol and distilled water, and dried with air.

3.6.2 Preparation of paste

3.6.2.1 TiO_2 paste

The TiO_2 paste 18NR–T was purchased from Dyesol and used without further preparation.

3.6.2.2 ZrO_2 paste

The paste used for ZrO_2 film preparation was prepared previous to the project by the PhD student Fredrik Johansson at the Chemistry and Chemical Engineering department at Chalmers University of Technology.

3.6.3 Preparation of films

3.6.3.1 TiO_2 films

Using the doctor blade method, a layer of TiO_2 paste was applied on the glass slide. In this method two stripes of Scotch tape are put on the sides of the glass slide, and a small amount of TiO_2 paste is applied to the non–taped area. The paste is spread out by pressing a glass rod towards the tape and pushing it along the slide. The thickness of the film becomes equal to the tape thickness which is approximately 6 µm. The films are then dried 30 min on a hot plate at 125°C, followed by a heating program in an oven.

3.6.3.2 ZrO_2 films

Before doctor blading, the ZrO_2 paste was stirred for 10 minutes using a magnetic stir bar. After this the doctor blade method was used to apply a layer of ZrO_2 paste on the glass slide, after which the films were dried. The doctor blading and drying of the films was carried out in the same way as with the TiO_2 films, described above.

3.6.4 Sintering of films

The films were gradually heated to 450°C and then sintered for 30 min using the temperature program in table 1. The oven was then turned off and the films allowed to cool down slowly.

Table 1: Temperature program used for the sintering of films.

Temperature (°C)	Time (min)
150	10
200	10
250	15
300	15
350	15
400	15
450	30

3.6.5 Film sensitization

3.6.5.1 TiO_2 films

To evaporate condensed water, the TiO_2 films were heated at 125°C on a hot plate for 15 minutes, after which the films were allowed to cool down for 10 minutes on the turned off hot plate. The films were then immersed for a minimum of 24 hours in a 0.1 mM solution of $[Ru(deeb)_2PyMeSO–iPr]^{2+}$ in CH_2Cl_2.

3.6.5.2 ZrO_2 films

To evaporate condensed water, the ZrO_2 films were heated at 150°C on a hot plate for 15 minutes, after which the films were allowed to cool down for 10 minutes on the turned off hot plate. The temperature was chosen to 150°C since a better adsorption was observed with higher temperature. The films were then immersed for a minimum of 24 hours in a 0.1 mM solution of $[Ru(deeb)_2PyMeSO–iPr]^{2+}$ in MeOH.

3.7 Determination of rate constants

In this project, rate constants have been determined by fitting the decay in absorbance to a monoexponential model, equation 4.

$$y = A*e^{-k*x} + y_0 \qquad \text{(eq. 4)}$$

where y_0 is the offset, A the amplitude and k a rate constant. If a monoexponential model did not produce satisfactory fittings, a biexponential model was used instead, equation 5.

$$y = A_1*e^{-k1*x} + A_2*e^{-k2*x} + y_0 \qquad \text{(eq. 5)}$$

4. Results and discussion

4.1 Photophysical and photochemical characterization of $[Ru(deeb)_2PyMeSO–iPr]^{2+}$ and $[Ru(deeb)_2PyMeS–iPr]^{2+}$

4.1.1 Ground state absorption

The absorption spectra of S–bonded $[Ru(deeb)_2PyMeSO–iPr]^{2+}$ in different solvents can be seen in figure 10A. The samples were prepared, kept and measured in the dark. In 10B the absorption spectrum is compared to $[Ru(deeb)_2PyMeS–iPr]^{2+}$ in PC.

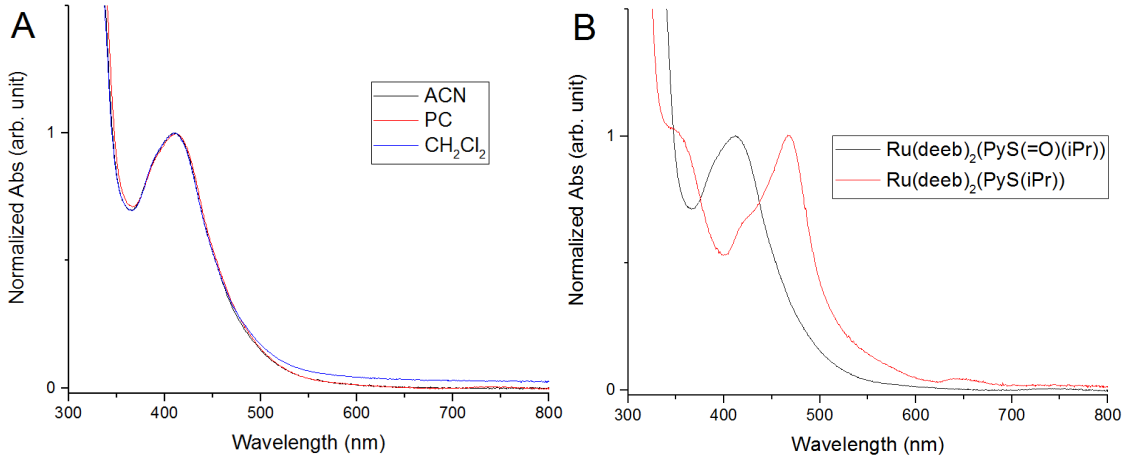

Figure 10: ***A)*** *Normalized absorbance for* $[Ru(deeb)_2PyMeSO–iPr]^{2+}$ *dissolved in ACN, PC and* CH_2Cl_2. ***B)*** *Normalized absorption spectra of* $[Ru(deeb)_2PyMeSO–iPr]^{2+}$ *and* $[Ru(deeb)_2PyMeS–iPr]^{2+}$ *in PC. The absorbances are normalized by* λ_{max} *of respective MLCT band.*

As the samples had not been exposed to light, figure 10A shows the absorption spectra of the thermodynamically stable S–bonded $[Ru(deeb)_2PyMeSO–iPr]^{2+}$. The band centered at 411 nm is interpreted as a MLCT transition, as MLCT in transition metal complexes generally occur at lowest energy for the smallest positive charge on the central metal ion [31]. The interpretation is supported by comparison with absorption spectrum of $[Ru(bpy)_2PyMeSO–iPr]^{2+}$, which displays an absorption spectrum of similar shape with a MLCT peak centered at 370 nm [37]. The redshift of the MLCT peak in $[Ru(deeb)_2PyMeSO–iPr]^{2+}$ relative $[Ru(bpy)_2PyMeSO–iPr]^{2+}$ can be explained by lower energies of the π^*_L–orbitals of deeb ligands resulting in a red shifted peak. The low energy of the deeb π^*_L–orbital is due to the electron withdrawing ester groups which stabilizes the excited state. The effect of the electron withdrawing esters is clearly seen in the comparison between $[Ru(bpy)_3]^{2+}$ displaying a 455 nm MLCT peak [12], and $[Ru(deeb)_3]^{2+}$ with a 465 nm MLCT peak [13].

Figure 10B shows the normalized ground state absorption of $[Ru(deeb)_2PyMeSO–iPr]^{2+}$ and corresponding thioether $[Ru(deeb)_2PyMeS–iPr]^{2+}$. $[Ru(deeb)_2PyMeSO–iPr]^{2+}$ has a peak at 411, while the thioether displays a shoulder at approximately 350 nm and peak at 468 nm. Thus in the corresponding thioether the lowest energy MLCT peak is red shifted to 468 nm, indicating stabilization of the MLCT excited state relative $[Ru(deeb)_2PyMeSO–iPr]^{2+}$. The result agrees with observations made by J.J. Rack where the MLCT peak was red–shifted in the thioether relative to the corresponding sulfoxide complex [38].

4.1.2 Photoinduced S– to –O isomerization

4.1.2.1 Photoinduced S– to –O isomerization in CH_2Cl_2 and PC

Figure 11A and 11B show the spectral response of $[Ru(deeb)_2PyMeSO–iPr]^{2+}$ to 385 nm irradiation in CH_2Cl_2 and PC, respectively. In CH_2Cl_2 peaks form at 371 nm and 500 nm. In PC peaks form at 374 and 503 nm. Simultaneous decrease in intensity at 411 nm is seen in both samples. Three maintained isosbestic points at 345, 397 and 440 nm in CH_2Cl_2 (346, 400 and 440 nm in PC) characterize the transition in both solvents.

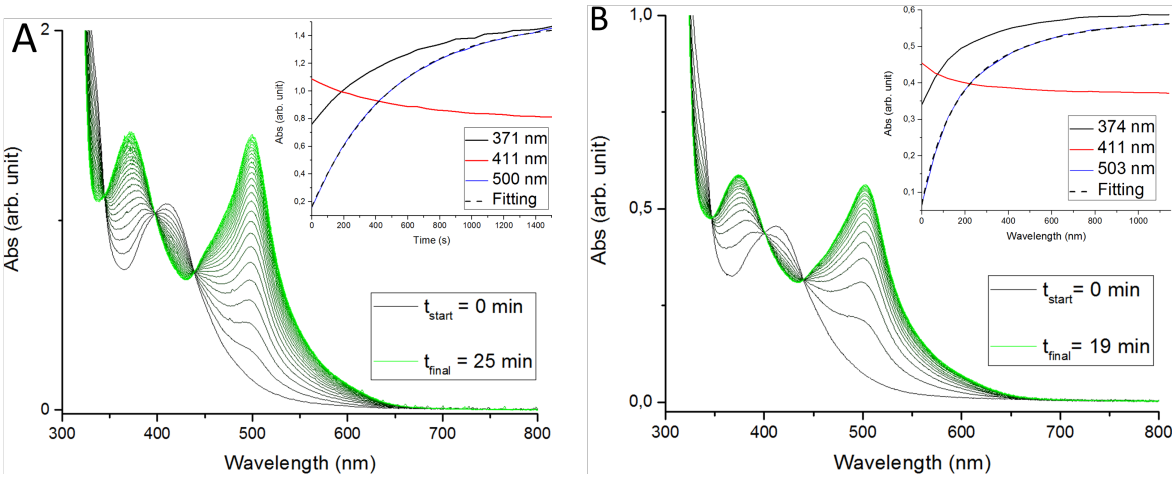

Figure 11: *$[Ru(deeb)_2PyMeSO–iPr]^{2+}$ in **A)** CH_2Cl_2 and **B)** PC is irradiated with 385 nm. Insets: Absorbance followed over time fitted to a **A)** monoexponential and **B)** biexponential model. Time between measurements: 1 min.*

The photochromic behavior in both solvents is interpreted as S– to– O isomerization, and the peak at ca 500 nm as MLCT excitation of the O–bonded form. Previous studies have shown that MLCT excitation of ruthenium sulfoxide complexes can induce isomerization from S–bonded to O–bonded sulfoxide ligand. For example, $[Ru(deeb)_2PyMeSO–iPr]^{2+}$ (bpy is 2,2'–bipyridine) excited by 370 nm results in isomerization from S– to O–bonded sulfoxide ligand, characterized by a rise of a peak at 472 nm due to O–bonded isomer MLCT [37]. The O–bonded MLCT peak in $[Ru(deeb)_2PyMeSO–iPr]^{2+}$ is expected to be red shifted relative to $[Ru(bpy)_2PyMeSO–iPr]^{2+}$ due

to lower energy π^*_L–orbitals due to deeb ligands. This is observed in our results with a MLCT peak located at 500 nm.

Comparing the S– to –O isomerization in CH_2Cl_2 and PC, the transition occurs with three maintained isosbestic points in both solvents, indicating a transition between two species without degradation or formation of byproduct. The O–bonded spectrum is slightly red shifted in PC while no shift is observed of the S–bonded spectrum. The kinetics are also different. S– to –O isomerization in CH_2Cl_2 was fitted to a monoexponential model with k= $2*10^{-3}$ s^{-1}, while kinetics in PC was fitted to a biexponential model with rate constants k_1= $1*10^{-2}$ s^{-1} and k_2= $3*10^{-3}$ s^{-1}.

4.1.2.2 Kinetic stabilization of O–bonded isomer in CH_2Cl_2

In figure 12 the achievable degree of photoinduced S– to –O isomerization is compared between solutions of $[Ru(deeb)_2PyMeSO–iPr]^{2+}$ in PC and CH_2Cl_2. By irradiation with 385 nm a photostationary state is reached. This absorption spectrum is then divided by the corresponding initial S–bonded absorption at 411 nm, in an attempt to correct for concentration differences.

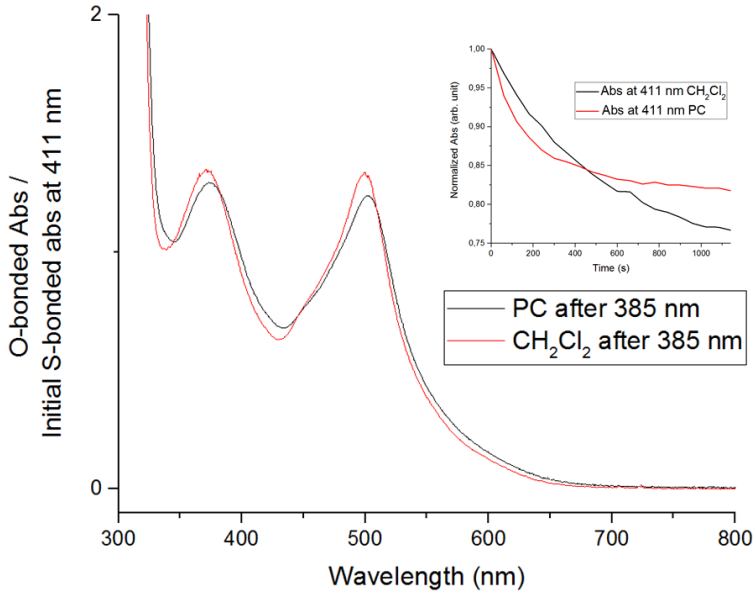

Figure 12: *Maximally isomerized absorption spectra of $[Ru(deeb)_2PyMeSO–iPr]^{2+}$ in PC and CH_2Cl_2. The absorbances are divided by their initial value of absorption at 411 nm.*
Inset: *Normalized absorbance at 411 nm over time as sample is irradiated by 385 nm.*

The spectrum observed in CH_2Cl_2 has a shape with higher absorbance at 371 and 500 nm relative to at 411 nm, which indicates a more S– to –O isomerized sample. This suggests a higher quantum yield for S– to –O isomerization in CH_2Cl_2. The inset shows that the absorbance

at 411 nm decreases to a higher degree in CH_2Cl_2 than in PC, corresponding to a higher degree of S– to –O isomerization. This again indicates a higher quantum yield for S– to –O isomerization in CH_2Cl_2.

4.1.3 Photoinduced O– to –S isomerization

Subsequent to 385 nm irradiation, $[Ru(deeb)_2PyMeSO–iPr]^{2+}$ in CH_2Cl_2 was irradiated with 623 nm. The spectral response can be seen in figure 13. The peak at 411 nm increases in intensity while peaks at 371 and 500 nm decrease in intensity. The transition occurs with maintained isosbestic points, and the spectrum is almost restored to its initial state.

4.1.3.1 Photoinduced O– to –S isomerization in CH_2Cl_2

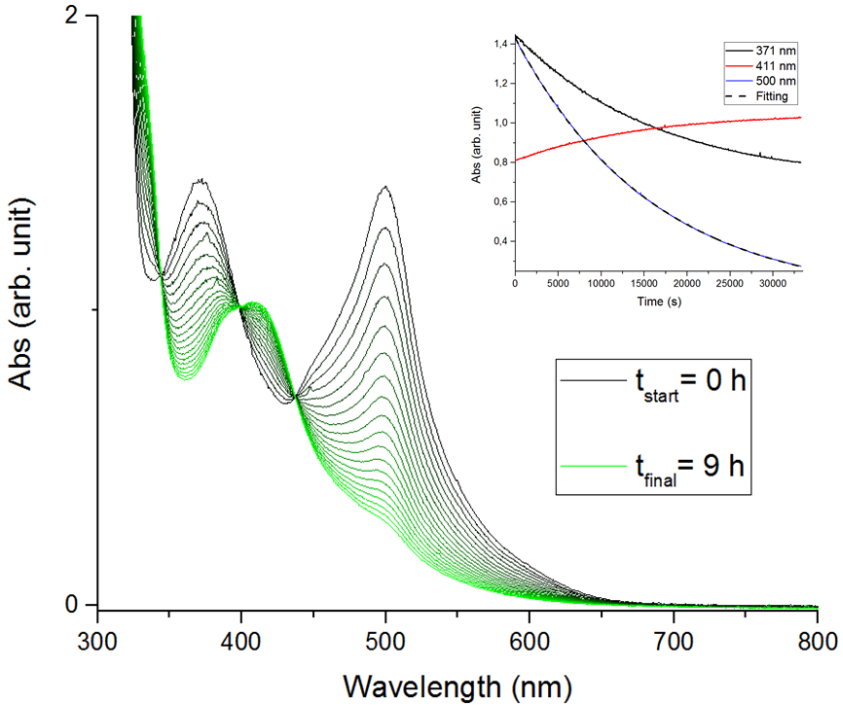

Figure 13: *$[Ru(deeb)_2PyMeSO–iPr]^{2+}$ in CH_2Cl_2 is irradiated with 623 nm after 385 nm irradiation.* ***Inset:*** *Absorbance followed over time fitted to a monoexponential model. Time between measurements: 30 min.*

By irradiating at 623 nm where only the O–bonded form absorbs, it was possible to excite only the O–bonded form, prompting O– to –S isomerization with little to no S–bonded absorption. Thus reversibility of S– to –O isomerization in $[Ru(deeb)_2PyMeSO–iPr]^{2+}$ is demonstrated. The maintained isosbestic points indicate a clean transition with no byproducts. In the final spectrum, a feature can be seen at 500 nm indicating a small concentration of O–bonded isomer in the sample.

4.1.4 Thermal decay O– to –S isomerization

4.1.4.1 Thermal decay in CH_2Cl_2 and PC

Figure 14A and 14C show the thermal decay of $[Ru(deeb)_2PyMeSO–iPr]^{2+}$ after 385 nm irradiation in CH_2Cl_2 and PC, respectively. In CH_2Cl_2 the decay is characterized by decreasing absorbance at 371 and 500 nm. In PC peaks at 378 and 503 peaks decrease in intensity. In both samples the intensity at 411 nm increases. Figure 14B and 14D shows the first hours of the process in CH_2Cl_2 and PC, respectively.

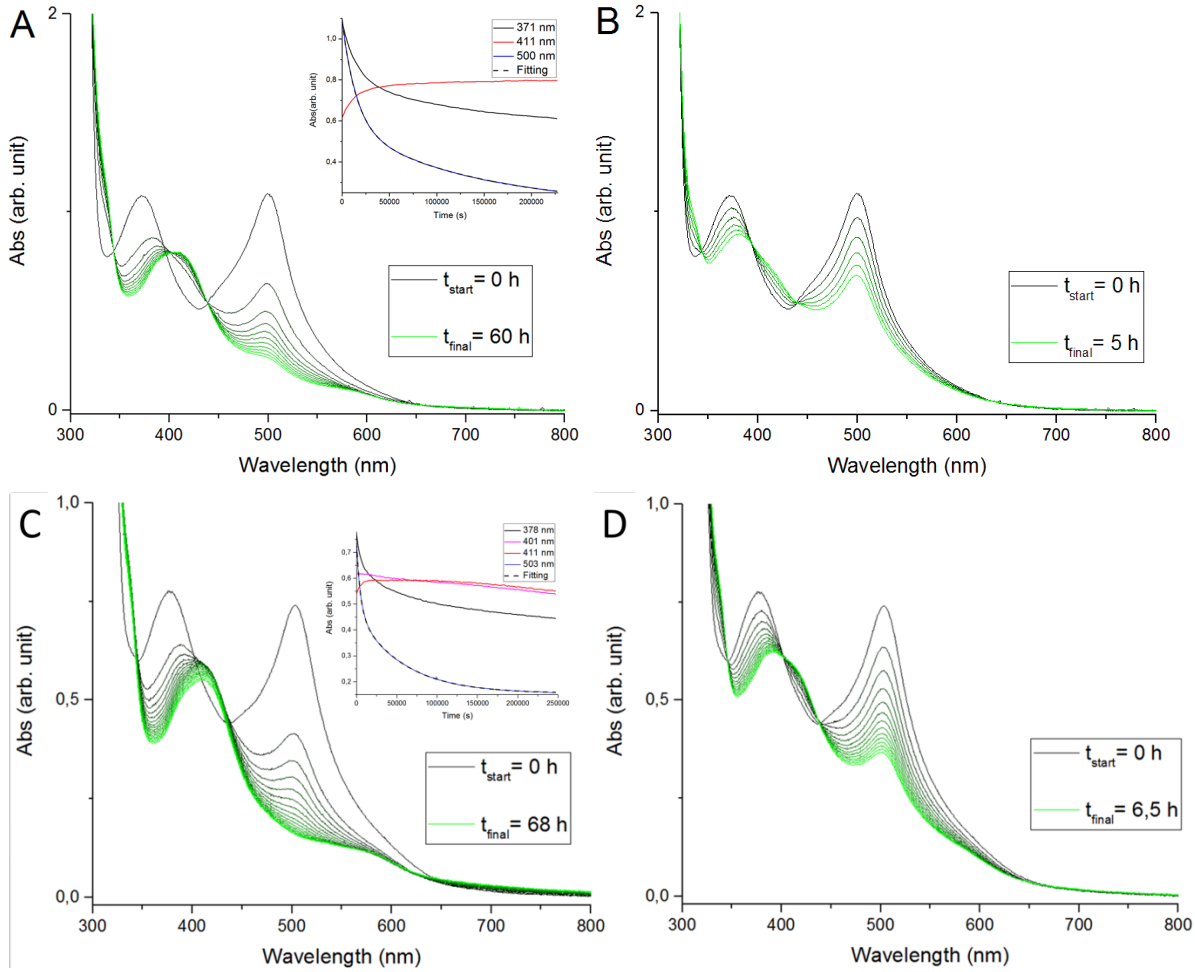

Figure 14: *Thermal decay of $[Ru(deeb)_2PyMeSO–iPr]^{2+}$ in **A)** CH_2Cl_2 and **C)** PC after 385 nm irradiation. The first hours of the processes is seen in **B)** CH_2Cl_2 and **D)** PC.*
***Insets:** Absorbance followed over time fitted to biexponential model. Time between measurements: **A)** 6 h **B)** 1 h **C)** 4 h **D)** 30 min.*

The spontaneous decrease in absorbance at ~370 and ~500 nm with simultaneous increase in absorbance at 411 nm is interpreted as O– to –S isomerization through thermal reversion. The thermal reversion is observed in both solvents. However, while three clear isosbestic points are maintained under the first hours, the isosbestic point at 398 nm (401 nm in PC) starts to shift

around 6 hours into the measurement. The change around the 398 nm isosbestic point is seen in both solvents, but is more pronounced in PC. In addition, a simultaneous formation of a peak at ~580 nm is observed in both solvents.

This behavior might be an indication of some byproduct formation under the transition. Another possibility is discussed by J.J. Rack and co–workers who studied thermal O– to –S reversion of $[Ru(bpy)_2(OSOBnF_5)]^{2+}$ ($OSOBnF_5$ = 2–pentafluorophenylmethanesulfinyl)benzoate) and found two sets of isosbestic points under the transition similar to our case. They proposed this to be due to two diastereomers of the O–bonded isomer with differing thermal reversion rates. The thermal reversion kinetics in their complex $[Ru(bpy)_2(OSOBnF_5)]^{2+}$ was described by a biexponential model, which is consistent with Racks theory [39]. In our project, the thermal reversion of $[Ru(deeb)_2PyMeSO–iPr]^{2+}$ is fitted to a biexponential model. This could indicate that Racks theory is correct and applicable to ruthenium sulfoxide complexes with deeb ligands. However more research is needed to find the origin of the changing isosbestic point.

4.1.5 Cyclic isomerization of $[Ru(deeb)_2PyMeSO–iPr]^{2+}$ in CH_2Cl_2

To investigate long term reversibility of isomerization, a sample of $[Ru(deeb)_2PyMeSO–iPr]^{2+}$ in CH_2Cl_2 previously isomerized and reversed was isomerized once more using 385 and consecutive 623 nm irradiation.

Figure 15 shows the spectral response of $[Ru(deeb)_2PyMeSO–iPr]^{2+}$ in CH_2Cl_2 being exposed to 385 nm and 623 nm irradiation for the second time. In figure 15A, 385 nm irradiation induces formation of peaks at 371 nm and 500 nm and a decrease of the 411 nm peak. A small feature in the ground state absorbance can be seen at ~580 nm from time zero. In 15B, 623 nm irradiation prompts intensity to increase at 411 nm and to decrease at 371 and 500 nm.
Maintained isosbestic points for both measurements indicate single transitions between two well–defined species.

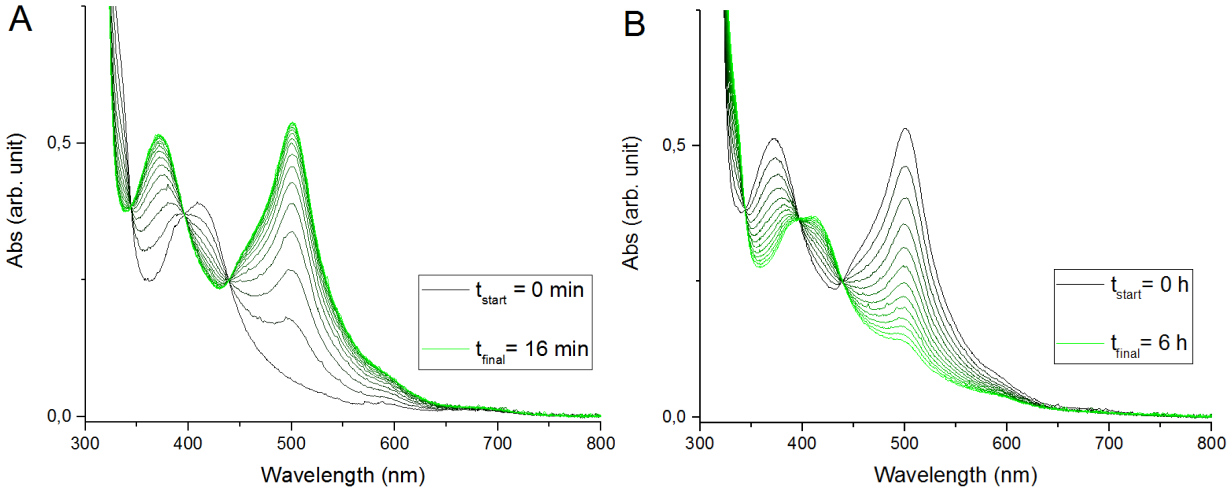

Figure 15: *Diluted $[Ru(deeb)_2PyMeSO–iPr]^{2+}$ in CH_2Cl_2 is irradiated with **A)** 385 nm followed by **B)** 623 nm. Time between measurements: 1 min and 30 min respectively.*

The photochromic behavior with the characteristic change between a 411 nm peak and two peaks at ~370 and ~500 nm is interpreted as S– to– O isomerization and reversion. In 15B the peak at 500 nm indicates that reversion is not as complete as in the first cycle, likely due to the difference in irradiation time between the first and second measurement (9 h vs 6 h). The 580 nm feature is still observed. Cyclic isomerization of the complex does not seem to damage the complex. While more cycles are required for a more reliable investigation of cyclability, it is an initial good sign.

In figure 15A at time zero a small feature is seen at ~580 nm. As it is present prior to 385 nm irradiation, this means it must have either been introduced either in the process of dilution or

that it is due to a chemical change which occurred under the four days between the first and second cycle.

4.1.6 Comparable experiments on the photochromic behavior of $[Ru(deeb)_2PyMeS–iPr]^{2+}$

4.1.6.1 Control of photostability in PC

Figure 16A and 16B show the spectrum of corresponding thioether $[Ru(deeb)_2PyMeS–iPr]^{2+}$ before and after irradiation with 385 and 460 nm, respectively. No change in the spectrum is observed.

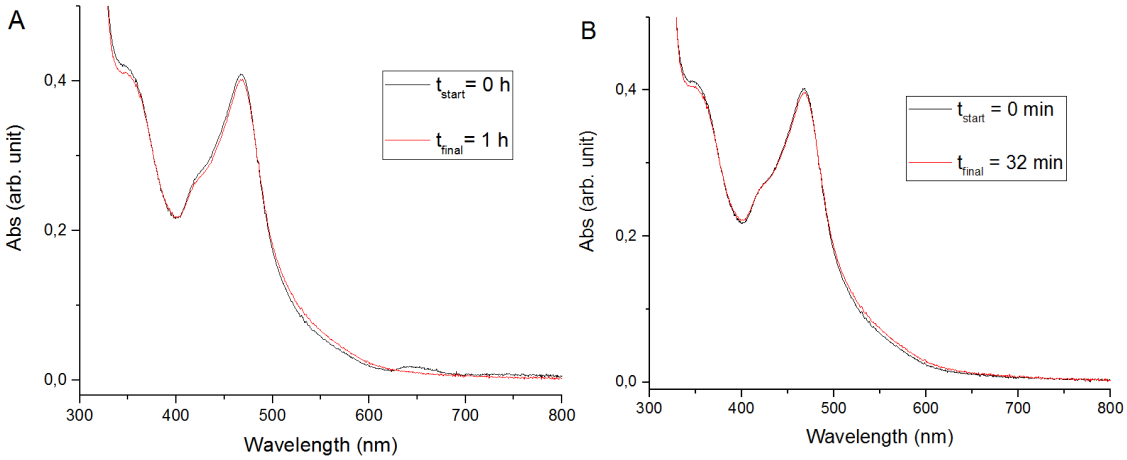

Figure 16: *$[Ru(deeb)_2PyMeS–iPr]^{2+}$ in PC is irradiated by **A)** 385 nm and **B)** 460 nm.*

Irradiation with 385 and 460 nm does not prompt photochromic behavior in corresponding thioether $[Ru(deeb)_2PyMeS–iPr]^{2+}$ in PC. The same result is obtained when performing the experiment in CH_2Cl_2. The lack of photochromism is explained by the absence of a sulfoxide group. The result is consistent with attributing photochromic behavior in $[Ru(deeb)_2PyMeSO–iPr]^{2+}$ to S– to –O isomerization.

4.2 Photoproduct formation

4.2.1 Photolysis of $[Ru(deeb)_2PyMeSO–iPr]^{2+}$ and $[Ru(deeb)_2PyMeS–iPr]^{2+}$ in ACN

Figure 17A shows the spectral response of $[Ru(deeb)_2PyMeSO–iPr]^{2+}$ in ACN to 385 nm irradiation, and 17B shows the first 5 minutes of the behavior. At first, peaks form at 364 and 460 nm and a decrease in the intensity for peak at 411 nm is observed. However, after the ~11-minute mark new peaks form at 343 and 452 nm while valleys form at 390 and 503 nm. Different isosbestic points are seen for both the initial and the later transition.

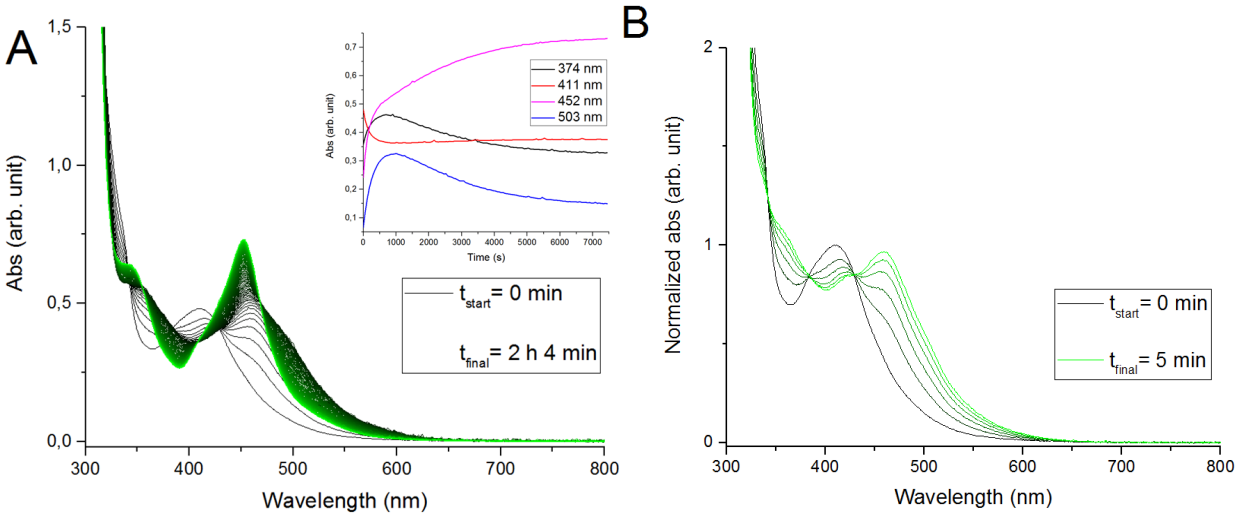

Figure 17: ***A)*** *$[Ru(deeb)_2PyMeSO–iPr]^{2+}$ in ACN spectral response to irradiation with 385 nm and* ***B)*** *The first 5 minutes of the behavior.* ***Inset:*** *Absorbance followed over time. Time between measurements: 1 min.*

The spectral evolution is interpreted as a two–step process, as two processes with separate isosbestic points were distinguished. This behavior differs from an S– to –O isomerization, and the absorption spectrum of the final product is different to that of the O–bonded isomer. However, it is possible that the initial behavior seen during the first 5 minutes (Fig. 17B) is an S– to –O isomerization, followed by another process which could be formation of a photoproduct. The process is light–induced, as it has been observed that $[Ru(deeb)_2PyMeSO–iPr]^{2+}$ in ACN is stable when protected from light (see Appendix 1).

Figure 18 shows the spectral response of corresponding thioether $[Ru(deeb)_2PyMeS–iPr]^{2+}$ in ACN under 385 nm irradiation. Formation of a valley at 391 nm and a peak at 453 nm is observed. The transition has two maintained isosbestic points indicating a single transformation between two species.

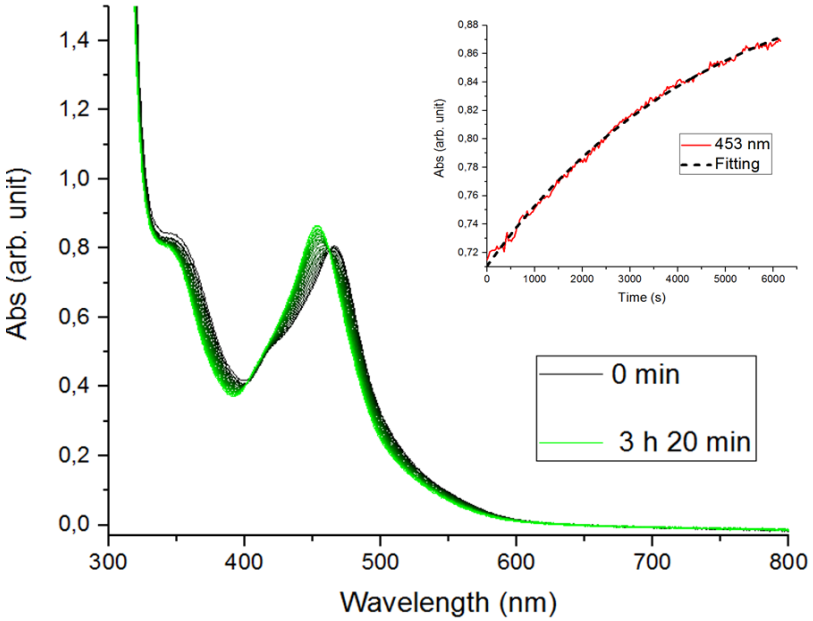

Figure 18: *[Ru(deeb)$_2$PyMeS–iPr]$^{2+}$ in ACN is irradiated with 385 nm.* ***Inset:*** *Absorbance followed over time fitted to a monoexponential model. Time between measurements: 10 min.*

[Ru(deeb)$_2$PyMeS–iPr]$^{2+}$ displays photochromic behavior in ACN, which is interesting since the thioether do not display photochromism in other solvents. This indicates that the formation of photoproduct is not dependent on an S– to –O isomerization mechanism.

4.2.2 Comparison of absorption spectra of photoproducts

The stability of the photoproducts formed in ACN is controlled by protecting the sample from light and monitoring the absorption spectrum. Figure 19A and 19B show photoproducts of [Ru(deeb)$_2$PyMeSO–iPr]$^{2+}$ and [Ru(deeb)$_2$PyMeS–iPr]$^{2+}$, respectively. In 19C the absorption spectra of the two photoproducts are compared.

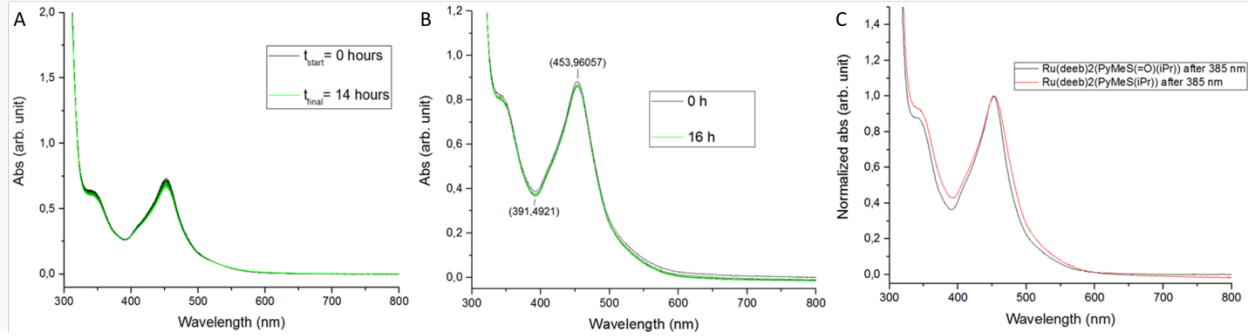

Figure 19: *The stability of formed photoproduct of* ***A)*** *[Ru(deeb)$_2$PyMeSO–iPr]$^{2+}$ and* ***B)*** *in ACN is controlled after irradiation with 385 nm.* ***C)*** *The spectra of the photoproducts. Time between measurements: 1 hour.*

In figures 19A and 19B a uniform decrease in absorption intensity is observed in both photoproducts. The uniform decrease indicates a decrease in photoproduct concentration, likely due to degradation. The shape of the spectra is however constant which indicates no further transitions and thus a stable photoproduct.

In figure 19C the two samples both display a valley at 391 nm and a peak at 452 nm, and the spectra have a similar shape, suggesting that $[Ru(deeb)_2PyMeSO–iPr]^{2+}$ and $[Ru(deeb)_2PyMeS–iPr]^{2+}$ to a large extent have formed the same product. However, the two spectra do not completely overlap, which might be explained by residual amounts of original complex due to non–complete conversion to photoproduct, or degradation during irradiation. In some ruthenium complexes, MLCT excitation can result in population of the ^{3}MC state which induces ligand exchange [34]. ACN is a coordinating solvent, and thus has the ability to coordinate to Ru(II) [40]. A reasonable explanation therefore is that MLCT excitation leads to replacement of one or more ligands by ACN molecules, but what ligands are uncertain. Logically, for the two different complexes to form the same product, the differing sulfur ligand must be exchanged in both complexes. In addition, it is possible deeb ligands are also replaced.

4.2.3 Comparison of emission spectra of photoproducts

Figure 20 shows the normalized emission spectrum of the photoproducts in response to 452 nm irradiation. The $[Ru(deeb)_2PyMeSO–iPr]^{2+}$ photoproduct displays peaks at 522 and 616 nm. The $[Ru(deeb)_2PyMeS–iPr]^{2+}$ photoproduct exhibits a peak at 624 nm.

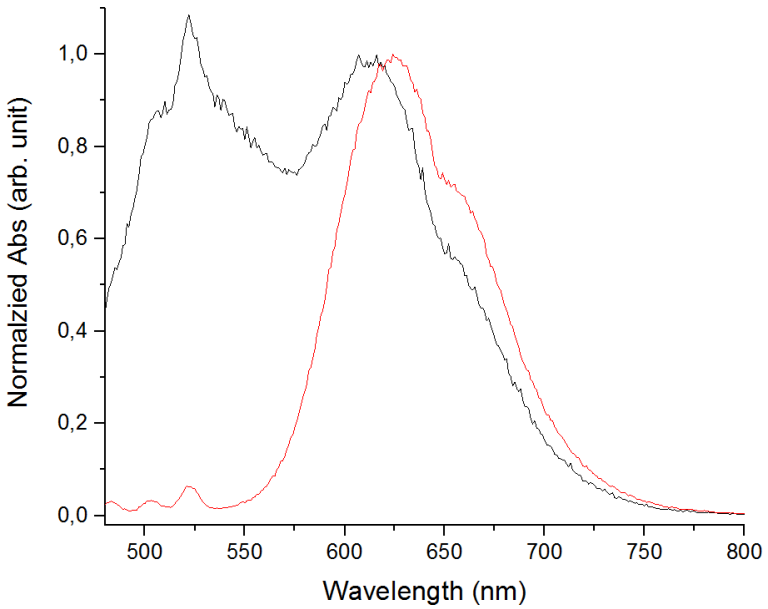

Figure 20: *Normalized emission spectra of formed photoproducts **black)** $[Ru(deeb)_2PyMeSO–iPr]^{2+}$ and **red)** $[Ru(deeb)_2PyMeS–iPr]^{2+}$ after irradiation with 385 nm in ACN. Excitation Wavelength: 452 nm.*

A peak at around 624 nm can be seen in both samples, which in both samples is assigned to MLCT emission from the deeb ligand, as deeb ligands in $[Ru(deeb)_3]^{2+}$ show an emission maximum at 626 nm [41]. Thus deeb ligand(s) seem to be part of both photoproducts. In the $[Ru(deeb)_2PyMeSO–iPr]^{2+}$ sample, an additional peak is observed at ~520 nm which could be unreacted or degraded original complex. In both samples a Raman peak at 525 nm due to the solvent can be seen. The shoulder at 655 nm in both samples is a known spectrophotometer artifact.

To investigate if the emission at ~620 nm originated from the same compound in both samples, the 625 nm excitation spectra were collected. Figure 21 shows the emission at 625 nm for the excitation wavelengths 400–500 nm. For $[Ru(deeb)_2PyMeSO–iPr]^{2+}$ two peaks are seen at 450 and 469 nm, while $[Ru(deeb)_2PyMeS–iPr]^{2+}$ displays a peak at 465 nm.

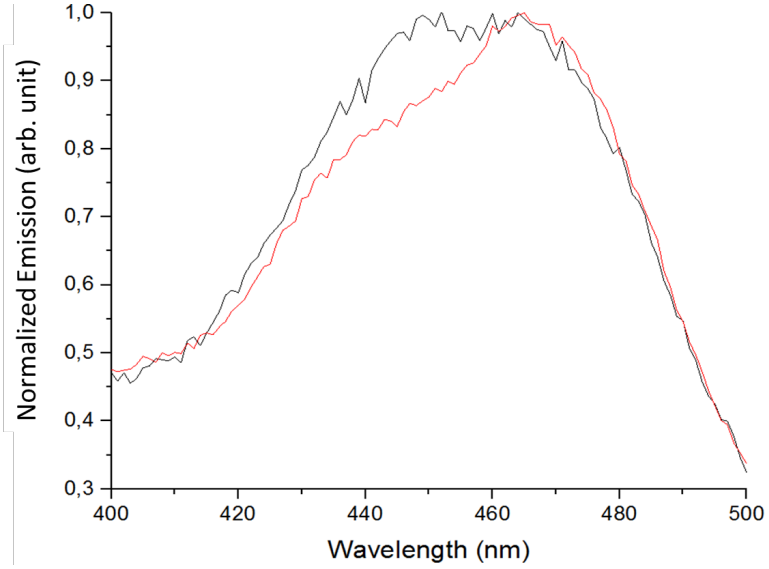

Figure 21: *Excitation spectra of **Black)** $[Ru(deeb)_2PyMeSO–iPr]^{2+}$ and **Red)** $[Ru(deeb)_2PyMeS–iPr]^{2+}$ after irradiation with 385 nm in ACN. Emission at 625 nm measured.*

Both samples show a peak around 465 nm, again indicating the presence of the same specie in both samples. However, in the $[Ru(deeb)_2PyMeSO–iPr]^{2+}$ sample a peak is also observed at 450 nm, indicating another specie which could be unreacted complex.

To investigate what caused emission at 525 nm in the two samples, the interval of excitation wavelengths 400–500 nm was scanned for emission at 525 nm. Figure 22 shows $[Ru(deeb)_2PyMeSO–iPr]^{2+}$ with features at 417 and 450 nm. The $[Ru(deeb)_2PyMeS–iPr]^{2+}$ sample did not display emission at 525 nm in response to these excitation wavelengths.

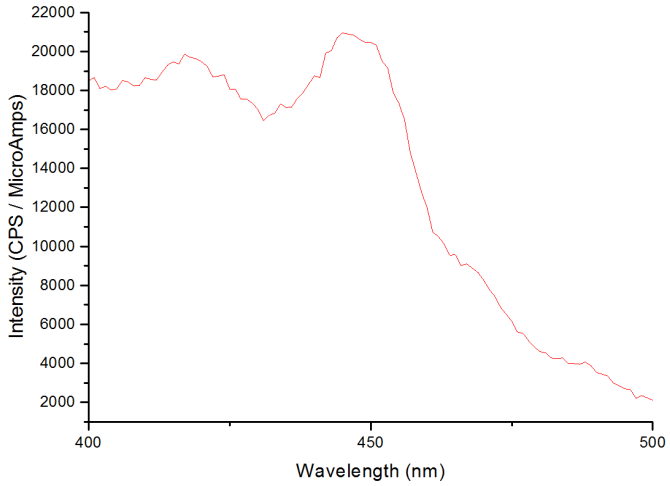

Figure 22: *Excitation of [Ru(deeb)$_2$PyMeSO–iPr]$^{2+}$ after irradiation with 385 nm in ACN. Emission at 525 nm measured.*

The emission observed in the [Ru(deeb)$_2$PyMeSO–iPr]$^{2+}$ sample which is not observed in the [Ru(deeb)$_2$PyMeS–iPr]$^{2+}$ sample, indicates the presence of a specie which is not present in the [Ru(deeb)$_2$PyMeSO–iPr]$^{2+}$ sample. This specie might be a degradation product or unreacted original complex.

In summary, there are indications that the photochemical reaction in ACN displayed by both [Ru(deeb)$_2$PyMeSO–iPr]$^{2+}$ and the corresponding thioether mainly forms the same product, probably with one or more deeb ligands. However the fact that the spectra of the two photoproducts do not completely overlap, and some emission displayed only in the [Ru(deeb)$_2$PyMeSO–iPr]$^{2+}$ sample, indicates presence of another specie, which could be degraded complex product or unreacted original complex.

4.3 Photochromic behavior of $[Ru(deeb)_2PyMeSO–iPr]^{2+}$ on TiO_2 and ZrO_2 mesoporous nanocrystalline thin films

By heating mesoporous nanocrystalline thin films of either TiO_2 or ZrO_2 and then immersing them in a solution of $[Ru(deeb)_2PyMeSO–iPr]^{2+}$ the complex was adsorbed on the surface. The photochromism of $[Ru(deeb)_2PyMeSO–iPr]^{2+}$ on film has been studied in air or immersed in solvents to see if potential solvent–dye or solvent–TiO_2 interaction impact photochromic behavior.

4.3.1 Photochromism of $[Ru(deeb)_2PyMeSO–iPr]^{2+}$ on TiO_2 films

4.3.1.1 Photoinduced S– to –O isomerization and thermal decay on TiO_2 in air

Figure 23A shows the absorbance spectrum of $[Ru(deeb)_2PyMeSO–iPr]^{2+}$ on TiO_2 in air initially, after 385 nm, and after thermal decay in the dark. 385 nm irradiation results in an absorbance increase at ~380 and 506 nm, while subsequent thermal decay prompts decreased intensity at 506 nm and increased intensity at ~380 nm. Figures 23B and 23C show absorbance at 506 nm versus time, during 385 nm and thermal decay respectively.

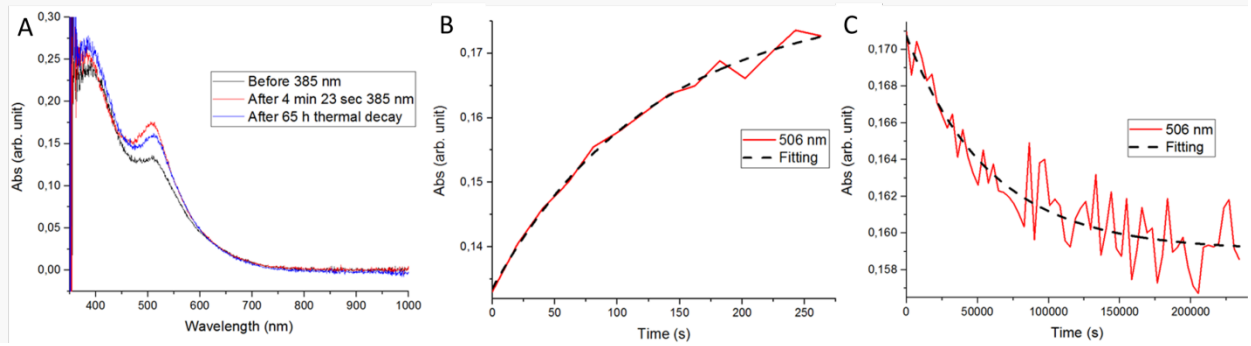

Figure 23: A) *TiO_2 film with adsorbed $[Ru(deeb)_2PyMeSO–iPr]^{2+}$ in **black)** initial state **red)** after 385 nm irradiation and **blue)** after thermal decay. **B)** Absorbance at 506 nm versus time during 385 nm irradiation fitted to monoexponential model. **C)** Absorbance at 506 nm versus time during 623 nm irradiation fitted to monoexponential model. The film is in air during the measurement.*

In 23A, a clear peak at 510 nm is observed in the initial spectrum, while no peak can be seen at around 411 nm where the S–bonded form absorbs strongly. This indicates adsorption of primarily O–bonded dye on this particular film. Initial adsorption of O–bonded form was sometimes observed after sensitization, which is peculiar since all films were immersed in solutions of initially S–bonded dye. There could be several reasons for the O–bonded adsorption, such as that O–bonded adsorption is favored, causing even small concentrations of the O–bonded form to bind in. Another possible explanation could be that dye baths isomerize

through a mechanism where dye molecules adsorb, isomerize, and desorb. As of now the actual reason for O–bonded adsorption is unknown. The O–bonded adsorption is discussed more in detail in section 4.3.3.

In response to 385 nm irradiation, peaks form at ~380 and 506 nm, indicative of an S– to –O isomerization. Thermal decay is observed, characterized by a decrease of intensity of the 506 nm peak. However contrary to the usually observed decrease in absorbance at ~380 nm during O– to–S isomerization, an increase in intensity at ~380 nm is seen. The increase of the ~380 nm peak both during 385 and 623 nm irradiation could be a change in the TiO_2 absorption spectrum, due to for example injected electrons or an electronic interaction with the dye.

4.3.1.2 Photoinduced S– to –O isomerization and photoinduced O– to –S reversion on TiO_2 in air and CH_2Cl_2

Figures 24A–C show $[Ru(deeb)_2PyMeSO–iPr]^{2+}$ on a TiO_2 film in air, while figures 30D–F show $[Ru(deeb)_2PyMeSO–iPr]^{2+}$ on a TiO_2 film in CH_2Cl_2. 24A and 24D show the absorbance spectrum of $[Ru(deeb)_2PyMeSO–iPr]^{2+}$ initially, after 385 nm, and after 623 nm irradiation. Figures 24B and 24E show absorbance versus time during 385 nm irradiation, and figures 24C and 24F show absorbance versus time during 623 nm irradiation.

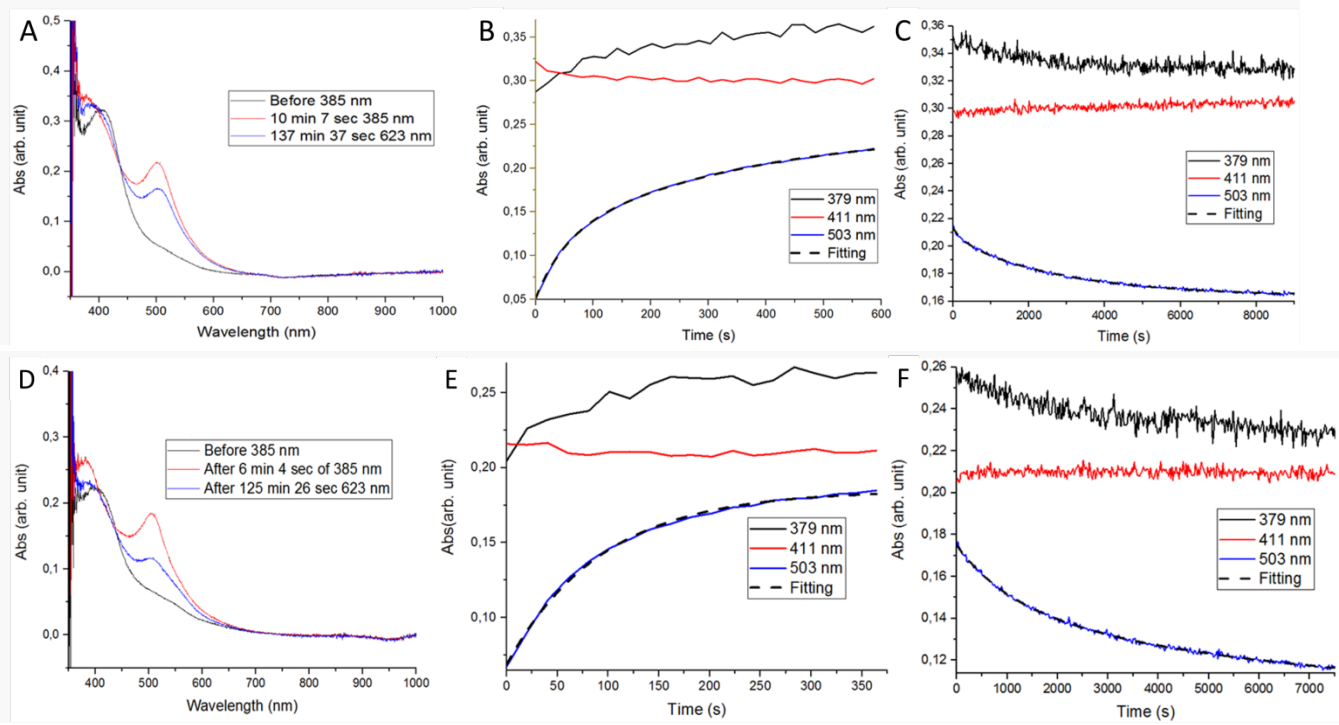

Figure 24: ***A–C)*** *TiO_2 film with adsorbed $[Ru(deeb)_2PyMeSO–iPr]^{2+}$ measured in air.*

A) *Absorption initially, after 385 nm and after thermal decay.* ***B)*** *Absorbance at 379, 411 and 506 nm versus time during 385 nm irradiation fitted to biexponential model. C) Absorbance at 379, 411 and 506 nm versus time during 623 nm irradiation fitted to a biexponential model.*

D–F) *TiO_2 film with adsorbed $[Ru(deeb)_2PyMeSO–iPr]^{2+}$ measured in CH_2Cl_2.*

D) *absorption initially, after 385 nm and after thermal decay.* ***E)*** *Absorbance at 379, 411 and 506 nm versus time during 385 nm irradiation fitted to monoexponential model.* ***F)*** *Absorbance at 379, 411 and 506 nm versus time during 623 nm irradiation fitted to a biexponential model.*

4.3.1.3 Photoinduced S– to –O isomerization and photoinduced O– to –S reversion on TiO_2 in PC

Figure 25 shows the absorbance spectrum of $[Ru(deeb)_2PyMeSO–iPr]^{2+}$ on TiO_2 in PC initially, after 385 nm, and after 623 nm irradiation. During the measurement a decrease in absorbance over the whole spectrum can be seen.

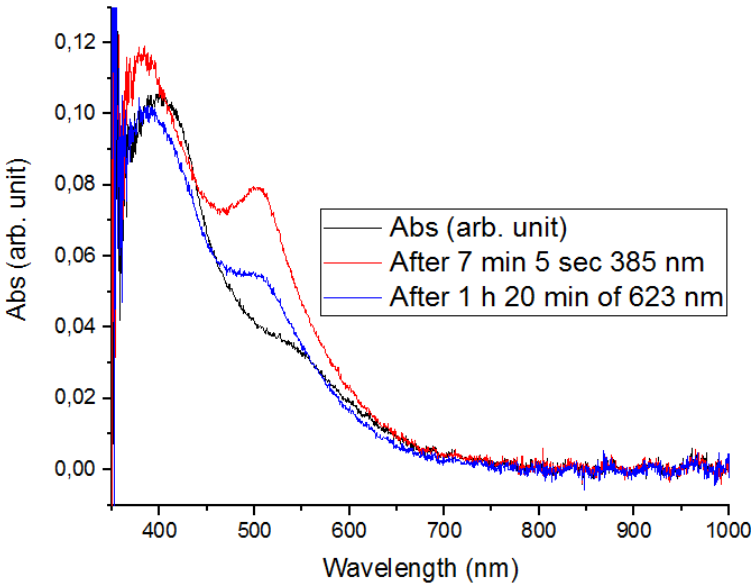

Figure 25: *TiO_2 film with adsorbed $[Ru(deeb)_2PyMeSO–iPr]^{2+}$ is irradiated with 385 nm followed by 623 nm. The film is in PC during the measurement.*

The initial absorption spectrum shows a somewhat isomerized $[Ru(deeb)_2PyMeSO–iPr]^{2+}$, indicated by the feature at ~500 nm. 385 nm irradiation results in absorbance increase at ~380 and 503 nm, while subsequent 623 nm prompts a large decrease in intensity at 503 nm. The photochromic behavior is thus interpreted as S– to –O isomerization and reversion. Over time the intensity of absorption decreases across the spectrum, indicating a lowering of dye concentration. This might be due to interaction between PC and TiO_2 which causes $[Ru(deeb)_2PyMeSO–iPr]^{2+}$ to desorb.

4.3.2 Photochromism of $[Ru(deeb)_2PyMeSO–iPr]^{2+}$ on ZrO_2 films

It was more difficult to adsorb $[Ru(deeb)_2PyMeSO–iPr]^{2+}$ on ZrO_2 than on TiO_2. The difference could be due to different electrostatic interactions between the dye and the two semiconductors, even though surface properties of TiO_2 and ZrO_2 has been found to be comparable [42]. Another possible explanation for the difference is the different solvents used for sensitization of the different films (CH_2Cl_2 for TiO_2 and MeOH for ZrO_2) which might affect interaction between the dye and the semiconductor. More experiments are required to determine the origin of the low adsorption on ZrO_2.

4.3.2.1 Photoinduced S– to –O isomerization and photoinduced O– to –S reversion in CH_2Cl_2

Figure 26 shows the absorbance spectrum of $[Ru(deeb)_2PyMeSO–iPr]^{2+}$ on ZrO_2 in CH_2Cl_2 initially, after 385 nm, and after 623 nm irradiation. After 623 nm irradiation, a decreased absorbance over the whole spectrum can be seen.

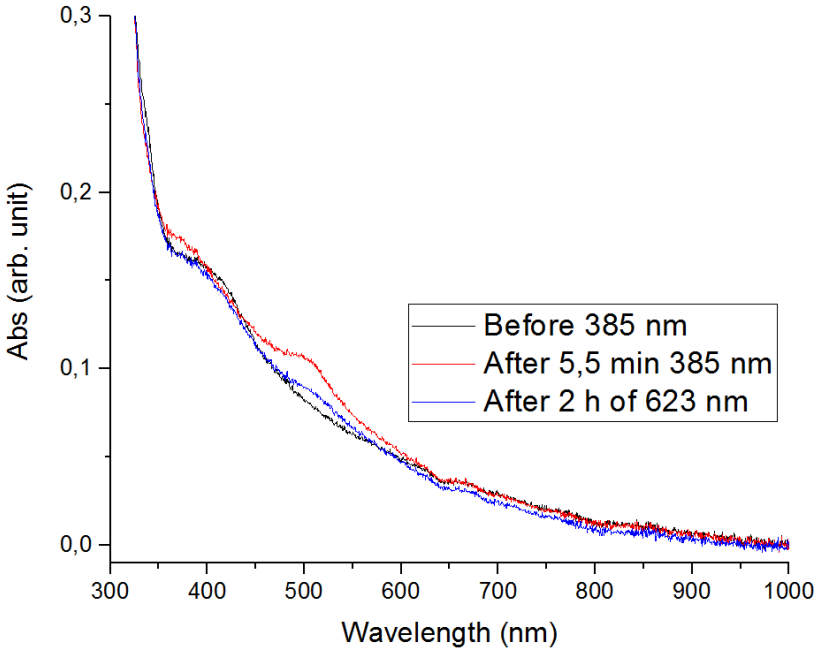

Figure 26: *ZrO_2 film with adsorbed $[Ru(deeb)_2PyMeSO–iPr]^{2+}$ is irradiated by 385 nm followed by 623 nm. The film is in CH_2Cl_2 during the measurement.*

The initial spectrum of the dye shows successful anchoring of dye on the ZrO_2, but with a mixed adsorption of S and O–bonded $[Ru(deeb)_2PyMeSO–iPr]^{2+}$. Low adsorption and adsorption of mostly O–bonded isomer was a common result for sensitized ZrO_2 films. 385 nm irradiation results in absorbance increase at ~380 and ~500 nm. With 623 nm the absorbance decreases at 500 nm and 380 nm towards the initial spectrum. The photochromic behavior is interpreted as S– to –O isomerization and reversion.

In the spectrum after 623 nm irradiation, absorbance is lowered across the spectrum. This is due to a known spectrophotometer artifact. Degradation of dye is not probable, since a decrease in absorbance is observed also in the 600+ region where the dye does not absorb.

4.3.3 Comments on the sensitization of thin films

In general, it was difficult to achieve high adsorption of $[Ru(deeb)_2PyMeSO–iPr]^{2+}$ to films. The highest absorption at 411 nm obtained was 0.3 on TiO_2, which is too low for doing for example transient absorption measurements. A consistent problem has been to selectively adsorb S–bonded $[Ru(deeb)_2PyMeSO–iPr]^{2+}$ on film. The reason for this is not certain, but a hypothesis is that the O–bonded adsorption is favored on TiO_2 and ZrO_2, causing even small concentrations of the O–bonded form to bind in. Another general observation is that solutions used as dye baths seem to isomerize more than other solutions. There might be a mechanism where the dye molecules adsorb, isomerize, and desorb. The source of the problem has not been identified, but from working with the coloring of the films a lot, it is most likely not due to some experimental error. It is more probable that it is chemically difficult to obtain only S–bonded isomer adsorption.

5. Kinetics comparison

In this section, the kinetics of the S– to –O isomerization and reversion in different environments are compared, mainly by analysis of the determined rate constants from the exponential fittings. The value of these rate constants can be influenced by experimental factors such as photon flux, sample concentration, the value of ε and the quantum yields of isomerization. In all measurements, the photon flux should have similar values since light intensity and distance between light source and sample was kept constant in all measurements. The concentrations have been varying between samples, with values of absorption at the MLCT peaks in $[Ru(deeb)_2PyMeSO–iPr]^{2+}$ and $[Ru(deeb)_2PyMeS–iPr]^{2+}$ between 0.45 –1.2. While ε of the S–bonded form is known, ε of the O–bonded form needs to be determined by for instance electrochemical measurements. Successful electrochemical measurements have not been achieved, which makes it difficult to determine the impact of ε on the rate constants. The quantum yields are complex to determine and this has not been attempted in the project.

5.1 Comparison of S– to –O isomerization rates

To compare the speed of the S– to –O isomerization in the different measurements, the rate constants from the exponential fittings are analyzed. The rate constants are showed in table 2. The ZrO_2 results are not included in this quantitative analysis due to too few experiments.

Table 2: All rate constants for S– to –O isomerization calculated during project.

Isomerization / Solvent	385 nm	385 nm on TiO_2
PC	$1*10^{-2}$ s^{-1} $3*10^{-3}$ s^{-1}	-
CH_2Cl_2	$2*10^{-3}$ s^{-1}	$1*10^{-3}$ s^{-1}
Air	-	$8*10^{-3}$ s^{-1}

One interesting observation is that the kinetics of the S– to –O isomerization differs in CH_2Cl_2 and PC. In PC the kinetics is fitted to a biexponential model while in CH_2Cl_2 the kinetics instead fits a monoexponential model. No clear difference in the speed of the isomerization in these two measurements can be determined from comparison of the rate constants. Another observed difference is that the S– to –O isomerization proceeds faster on TiO_2 in air than on TiO_2 in CH_2Cl_2 by almost one order of magnitude.

5.2 Comparison of O– to –S reversion rates

Irradiation with 623 nm and thermal decay have been ways of obtaining O– to –S reversion. In addition, irradiation with 523 nm was initially used for photoinduced reversion. In this section the extent of reversion of the three methods are discussed in different solvents or on mesoporous nanocrystalline thin films of TiO_2. The ZrO_2 results are not included in this quantitative analysis due to too few experiments.

Figure 27 shows the final spectra of $[Ru(deeb)_2PyMeSO–iPr]^{2+}$ in CH_2Cl_2 reversed by 523 nm irradiation, 623 nm irradiation, and thermal decay. All the final spectra have been normalized by division with the corresponding initial S-bonded absorption at 411 nm.

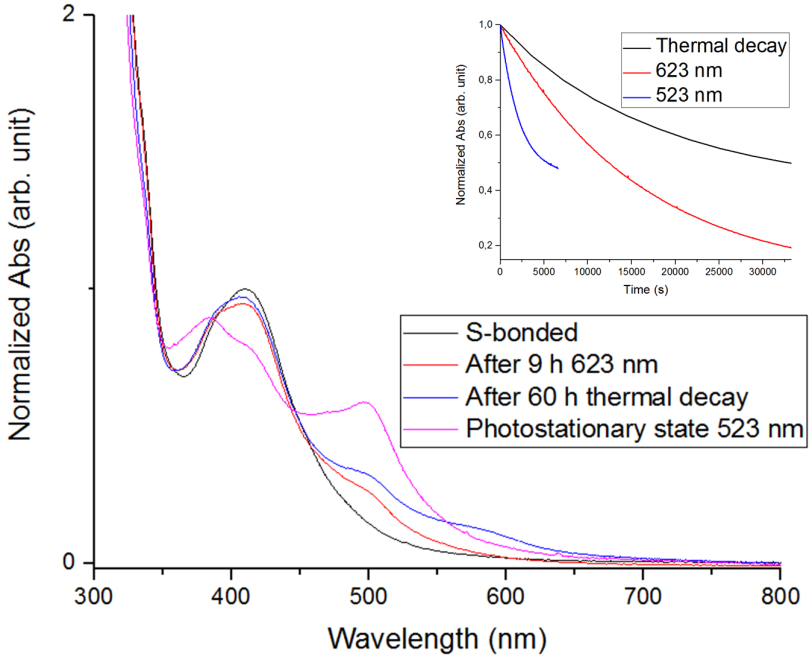

Figure 27: ***Black)*** *Initial S–bonded* $[Ru(deeb)_2PyMeSO–iPr]^{2+}$ ***Red)*** *after 385 nm followed by 623 nm* ***Pink)*** *after 385 nm followed by 523 nm and* ***Blue)*** *after 385 nm followed by thermal reversion. All samples were dissolved in* CH_2Cl_2. ***Inset:*** *Absorbance at 500 nm followed over time for the thermal decay, 623 and 523 nm irradiation.*

Inspection of the 450–750 nm interval shows that irradiating 623 nm for 9 hours results in a nearly complete reversion. The reversion is fast compared to thermal decay which did not transition back to the same degree over 60 hours. Irradiation with 523 nm isomerizes the sample fast initially compared to 623 nm, but after approximately 110 minutes a photostationary state is reached and more irradiation causes degradation of sample. The faster isomerization rate at 523 nm might be due to the higher molar absorptivity of the O–bonded form at this wavelength. The results indicate that 623 nm is a suitable wavelength for selective O– to –S isomerization in $[Ru(deeb)_2PyMeSO–iPr]^{2+}$. The photoinduced O– to –S isomerization

with both 523 and 623 nm irradiation were fitted to monoexponential models while thermal decay was fitted to a biexponential model.

Table 3: All rate constants for O– to –S isomerization calculated during project.

Reversion / Solvent	623 nm photoinduced	523 nm photoinduced	Thermal decay	623 nm on TiO_2	Thermal on TiO_2
PC	-	$5*10^{-3}$ s^{-1} $3*10^{-4}$ s^{-1}	$2*10^{-4}$ s^{-1} $2*10^{-5}$ s^{-1}	-	-
CH_2Cl_2	$6*10^{-5}$ s^{-1}	$5*10^{-4}$ s^{-1}	$7*10^{-5}$ s^{-1} $7*10^{-6}$ s^{-1}	$1*10^{-3}$ s^{-1} $2*10^{-4}$ s^{-1}	-
Air	-	-	-	$3*10^{-3}$ s^{-1} $3*10^{-4}$ s^{-1}	$2*10^{-5}$ s^{-1}

Comparison of rate constants in table 3 results in some meaningful insights. First, reversion with 523 nm is faster than 623 nm. This should not be a concentration effect, as the concentration of the sample was higher in the 623 nm measurement than in the 523 nm measurement. However, it is very likely that the much higher value of ε at 523 nm compared to 623 nm influenced the determined rate constants.

Secondly, both photoinduced 523 and 623 nm reversion is faster than thermal decay. The absorbance values at 411 nm in the initial samples are 0.55, 1.1 and 0.82 in the 523 nm, 623 nm and thermal reversion respectively. As the concentration is the lowest in the 523 nm measurement and this is still faster than thermal reversion, this is not a concentration effect. The 623 nm sample however has ~twice as high concentration as the thermal reversion sample, which might lead to misleadingly high rate constant values.

In addition, O– to –S isomerization is faster in PC than in CH_2Cl_2, indicating a kinetic stabilization of the O–bonded isomer in CH_2Cl_2 relative to PC. This is consistent with what was seen in section 4.1.2.2 where the S– to –O isomerization comes longer in CH_2Cl_2. However, the concentration is somewhat higher in the CH_2Cl_2 sample which might have affected the rate constants. The difference in concentration between the samples is seen from the 411 nm absorption of their corresponding S–bonded spectra; 0.55 at 411 nm in CH_2Cl_2 compared to 0.65 in PC which might be enough to influence the values of the determined rate constants.

Initial reversion is faster on TiO_2 film immersed in CH_2Cl_2 than in CH_2Cl_2 solution. This again indicates a kinetic stabilization of the O–bonded form in CH_2Cl_2, relative to on TiO_2 film in CH_2Cl_2.

The O– to –S isomerization is a little faster on a TiO_2 film in air compared to a film in CH_2Cl_2, once again indicating some kinetic stabilization of the O–bonded form in CH_2Cl_2. A possible explanation for this is that solvent molecules can reorganize around the isomerized specie which increases the lifetime of the O–bonded form. However the higher value of the rate constant in air, might be due to the higher concentration of $[Ru(deeb)_2PyMeSO–iPr]^{2+}$ on the film in air. More experiments on films with equal adsorption are needed to support this observation.

6. Conclusions and future outlook

In conclusion, the photochromism of $[Ru(deeb)_2PyMeSO–iPr]^{2+}$ has been investigated. In non–coordinating solvents reversible S– to –O isomerization is observed. Close to complete photoinduced O– to –S reversion is possible with irradiation of 623 nm. If instead the O–bonded form is irradiated with 523 nm, reversion is observed but results in a photostationary state. However with 523 nm the initial reversion is faster than with 623 nm.

O–bonded $[Ru(deeb)_2PyMeSO–iPr]^{2+}$ is demonstrated to spontaneously transition to S–bonded through thermal reversion. In all solvents and on film the thermal reversion is slower than photoinduced reversion. O– to –S isomerization is faster in PC than in CH_2Cl_2, indicating a kinetic stabilization of the O–bonded isomer in CH_2Cl_2 relative to PC.

MLCT excitation of $[Ru(deeb)_2PyMeSO–iPr]^{2+}$ in coordinating solvent ACN results in formation of a photoproduct, while $[Ru(deeb)_2PyMeSO–iPr]^{2+}$ in ACN kept in the dark is stable. This is possibly explained by MLCT irradiation resulting in population of ^{3}MC state leading to cleaving of Ru–ligand bonds, followed by coordination of ACN molecules to ruthenium(II).

Adsorption of $[Ru(deeb)_2PyMeSO–iPr]^{2+}$ to TiO_2 and ZrO_2 films is demonstrated, however the extent of adsorption is lower than desired for ultra–fast transient absorption spectroscopy. S– to –O isomerization and reversion is demonstrated on both TiO_2 and ZrO_2 films. Reversion of O–bonded $[Ru(deeb)_2PyMeSO–iPr]^{2+}$ adsorbed on TiO_2 is slower in CH_2Cl_2 than in air. A possible explanation for this is rearrangement by the solvent which stabilizes the O–bonded state.

Future work that would be desired is the determination of isomerization quantum yields and redox properties of the two isomers, study redox properties of dye and investigate if S and O–bonded isomers have different properties. For quantum yields the individual extinction coefficients of the S–bonded and O–bonded form need to be determined by electrochemical measurements.

An important goal is to find out optimal parameters during the sensitization process such as concentration, sensitization time, solvent, and temperature of immersed films to achieve higher adsorption. Higher adsorption brings signal to noise ratio up which would be welcome in photolysis measurements and needed in ultra–fast transient absorption spectroscopy.

Acknowledgements

First I want to thank Elin who supervised my project despite being a fresh Ph. D. with many irons in the fire. Your hard–working nature and kind and easy–going personality made it a pleasure to work together.

I want to thank Maria for the opportunity to work in the academia, and to learn more about solar technology which interests me deeply. The guidance and depth of knowledge you brought to the table was very impressing. Your personality and leadership was a large part of what made this project a great experience.

At last I want to thank everyone else that helped me. Many were you who happily helped me with small or big problems. I also met many people which I now consider friends. You contributed to great memories.

To all mentioned above, a big thank you. I wish you the best of luck in the future.

Appendix

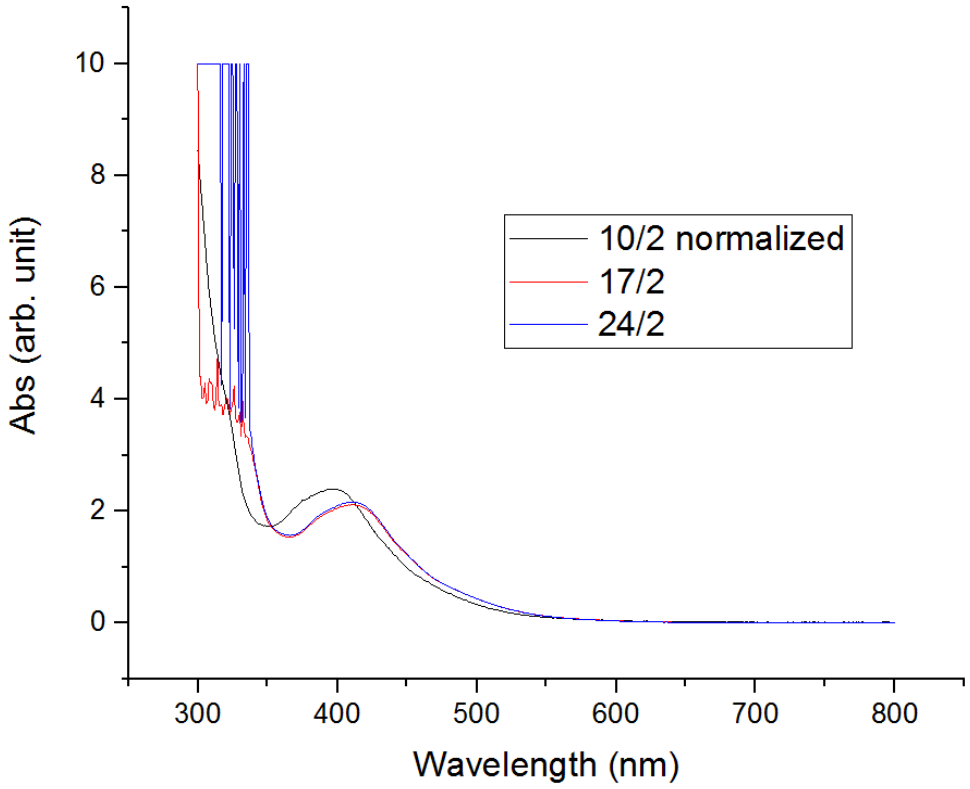

Appendix 1: *The stability of light protected* $[Ru(deeb)_2PyMeSO–iPr]^{2+}$ *in ACN is controlled over three weeks. The blue shifted initial spectrum is shifted due to uncalibrated spectrophotometer.*

References

[1] W. R. L. Anderegg, J. W. Prall, J. Harold, and S. H. Schneider, “Expert credibility in climate change,” vol. 107, no. 27, pp. 12107–12109, 2010.

[2] M. Grätzel, “Dye-sensitized solar cells,” vol. 4, pp. 145–153, 2003.

[3] T. J. Meyer, M. K. Brennaman, R. J. Dillon, L. Alibabaei, M. K. Gish, C. J. Dares, D. L. Ashford, R. L. House, G. J. Meyer, and J. M. Papanikolas, “Finding the Way to Solar Fuels with Dye-Sensitized Photoelectrosynthesis Cells,” *J. Am. Chem. Soc.*, vol. 138, no. 40, pp. 13085–13102, 2016.

[4] A. Hagfeldt, G. Boschloo, L. Sun, L. Kloo, and H. Pettersson, “Dye-Sensitized Solar Cells,” pp. 6595–6663, 2010.

[5] V. Balzani and A. Juris, “Ru(II) Polypyridine Complexes: Photophysics, Photochemistry, Electrochemistry, and Chemiluminescence,” *Coord. Chem. Rev.*, vol. 84, pp. 85–277, 1988.

[6] K. Nakamaru, “Synthesis, Luminescence Quantum Yields, and Lifetimes of Trischelated Ruthenium(II) Mixed-ligand Complexes Including 3,3’-Dimethyl-2,2’-bipyridyl,” *Bull. Chem. Soc. Jpn.*, vol. 55, no. 9, pp. 2697–2705, 1981.

[7] A. J. Thomson, V. Skarda, M. J. Cook, A. P. Lewis, G. S. G. Mcauliffe, and D. J. Robbins, “Luminescent Metal Complexes. Part 3.’ Electrochemical Potentials of Ground and Excited States,” *J. Chem. Soc. Perkin Trans. 2*, vol. 55, pp. 1309–1311, 1984.

[8] T. J. Meyer, D. L. Ashford, C. R. K. Glasson, M. R. Norris, J. J. Concepcion, S. Keinan, M. K. Brennaman, and J. L. Templeton, “Controlling Ground and Excited State Properties through Ligand Changes in Ruthenium Polypyridyl Complexes,” *Inorg. Chem.*, vol. 53, pp. 5637–5646, 2014.

[9] H. Taube, N. Scott, and A. Yeh, “S to 0 and 0 to S Linkage Isomerization in Sulfoxide Complexes of Pentaammineruthenium,” *Inorg. Chem.*, vol. 21, no. 7, pp. 2542–2545, 1982.

[10] L. Roecker, J. C. Dobson, W. J. Vining, and T. J. Meyer, “Oxygen atom transfer in the oxidations of dimethyl sulfide and dimethyl sulfoxide by bis(bipyridine)oxo(pyridine) ruthenium(2+),” *Inorg. Chem.*, vol. 26, no. 5, pp. 779–781, 1987.

[11] J. Rack, A. W. King, and L. Wang, “Excited State Dynamics and Isomerization in Ruthenium Sulfoxide Complexes,” 2015.

[12] G. G. Malliaras, K. W. Lee, J. D. Slinker, A. A. Gorodetsky, H. D. Abrun, and P. L. Houston, “Photophysical properties of tris(bipyridyl)ruthenium(,” no. 150 ml, pp. 10–13, 2003.

[13] G. J. Meyer, Z. Chen, J. J. Concepcion, T. J. Meyer, G. J. Hutchings, B. H. Farnum, J. M. Gardner, A. Marton, and A. A. Narducci-sarjeant, “Influence of ion pairing on the oxidation of iodide by MLCT excited states,” *Dalt. Trans.*, vol. 40, no. 15, pp. 3830–3838, 2011.

[14] P. Atkins and L. Jones, *Chemical Principles: The quest for insight*, 5th ed. New York: W.H. Freeman, 2010.

[15] J. M. Hollas, *Modern Spectroscopy*, 4th Editio. Chichester: John Wiley and Sons, Ltd, 2010.

[16] F. Rioux, “Hund ’ s Multiplicity Rule Revisited,” vol. 84, no. 2, pp. 358–360, 2007.

[17] Y. et al. Tanaka, “Impact of near-infrared radiation in dermatology,” *World*, vol. 1, no. 3, pp. 30–37, 2012.

[18] P. Atkins, T. Overton, J. Rourke, M. Weller, and F. Armstrong, *Shriver and Atkins’ Inorganic Chemistry.*, 5th ed. Oxford University Press, 2010.

[19] J. R. Lakowicz, *Principles of fluorescence spectroscopy*. Springer Science & Business Media, 2013.

[20] V. S. Becerril, “Studies of Charge Separation in Molecular and Molecular- Inorganic materials Assemblies for Solar Energy Conversion,” 2015.

[21] M. Grätzel and B. O’Regan, “A low cost, high efficiency solar cell based on dye-sensitized colloidal TiO2 films,” *Nature*, vol. 353, no. 24, pp. 737–740, 1991.

[22] M. K. Nazeeruddin, A. Kay, E. Miiller, P. Liska, N. Vlachopoulos, M. Gratzel, C.- Lausanne, and R. April, “Conversion of Light to Electricity by cis-X2Bis(2,2’-bipyridyl-4,4’-dicarboxylate)ruthenium(II)Charge-Transfer Sensitizers (X = Cl-, Br-, I-, CN-, and SCN-) on Nanocrystalline Ti02 Electrodes,” *Am. Chem. Soc.*, vol. 115, no. 14, pp. 6382–6390, 1993.

[23] M. Grätzel, K. Nazeeruddin, and P. Péchy, “Efficient panchromatic sensitization of nanocrystalline TiO 2 films by a black dye based on a trithiocyanato – ruthenium complex,” *Chem. Commun.*, vol. 1, no. 18, pp. 1705–1706, 1997.

[24] H. Arakawa, K. Hara, H. Sugihara, Y. Tachibana, A. Islam, M. Yanagida, and K. Sayama, “Dye-Sensitized Nanocrystalline TiO2 Solar Cells Based on Ruthenium (II) Phenanthroline Complex Photosensitizers,” *Am. Chem. Soc.*, vol. 17, no. 19, pp. 5992–5999, 2001.

[25] E. Palomares, A. Reynal, A. Forneli, E. Martinez-ferrero, A. Sanchez-diaz, and A. Vidal-ferran, “A Phenanthroline Heteroleptic Ruthenium Complex and Its Application to Dye-Sensitised Solar Cells,” *Eur. J. Inorg. Chem.*, pp. 1955–1958, 2008.

[26] J. B. Goodenough, S. Anderson, E. C. Constable, A. Hamnett, K. R. Seddon, and R. D. Wright, “Chemical modification of a titanium(IV) oxide electrode to give stable dye sensitisation without a supersensitiser,” *Nature*, vol. 280, no. 16, pp. 571–573, 1979.

[27] M. Grätzel, P. Wang, and S. M. Zakeeruddin, “High efficiency dye-sensitized nanocrystalline solar cells based on ionic liquid polymer gel electrolyte,” *Chem. Commun.*, vol. 5, pp. 2972–2973, 2002.

[28] M. Grätzel, C. Barolo, K. Nazeeruddin, S. Fantacci, D. Di Censo, P. Comte, P. Liska, G. Viscardi, P. Quagliotto, F. De Angelis, and S. Ito, “Synthesis , Characterization , and DFT-TDDFT Computational Study of a Ruthenium Complex Containing a Functionalized Tetradentate Ligand,” *Inorg. Chem.*, vol. 45, no. 12, pp. 4642–4653, 2006.

[29] S. A. Haque, S. Handa, K. Peter, E. Palomares, M. Thelakkat, and J. R. Durrant, “Supermolecular Control of Charge Transfer in Dye-Sensitized Nanocrystalline TiO2 Films: Towards a Quantitative Structure-Function Relationship,” *Angew. Chemie Int. Ed.*, vol. 44, pp. 5740–5744, 2005.

[30] D. Rehm and A. Weller, “Kinetics of fluorescence quenching by electron and H-atom transfer,” *Isr. J. Chem.*, vol. 8, no. 2, pp. 259–271, 1970.

[31] H. B. Gray, “Molecular Orbital Theory for Transition Metal Complexes,” *J. Chem. Educ.*, vol. 41, no. 1, pp. 2–12, 1964.

[32] T. J. Meyer, D. W. Thompson, and A. Ito, “[Ru(bpy)3]2+ and other remarkable metal-to-ligand charge transfer (MLCT) excited states,” *Pure Appl. Chem.*, vol. 85, no. 7, pp. 1257–1305, 2013.

[33] G. S. Hanan and E. A. Medlycott, “Designing tridentate ligands for ruthenium(II) complexes with prolonged room temperature luminescence lifetimes,” *Chem. Soc. Rev.*, vol. 34, pp. 133–142, 2005.

[34] J. V Caspar and T. J. Meyer, “Photochemistry of MLCT Excited States. Effect of Nonchromophoric Ligand Variations on Photophysical Properties in the Series,” *Am. Chem. Soc.*, vol. 22, no. 17, pp. 2444–2453, 1983.

[35] M. Abrahamsson, *Tuning of the Excited State Properties of Ruthenium (II) - Polypyridyl Complexes*, no. Ii. 2006.

[36] D. G. Brown, N. Sanguantrakun, B. Schulze, U. S. Schubert, and C. P. Berlinguette, “Bis(tridentate) Ruthenium−Terpyridine Complexes Featuring Microsecond Excited-State Lifetimes,” *J. Am. Chem. Soc.*, vol. 134, pp. 12354–12357, 2012.

[37] J. J. Rack and B. A. Mcclure, “Two-Color Reversible Switching in a Photochromic Ruthenium Sulfoxide Complex **,” pp. 8556–8558, 2009.

[38] D. P. Butcher, A. A. Rachford, J. L. Petersen, J. J. Rack, C. E. Bennett, W. Virginia, V. Uni, and W. Virginia, “Phototriggered S- to -O Isomerization of a Ruthenium-Bound Chelating Sulfoxide,” *Inorg. Chem.*, vol. 45, no. 23, pp. 2432–2433, 2006.

[39] J. J. Rack, B. A. Mcclure, and E. R. Abrams, “Excited State Distortion in Photochromic Ruthenium Sulfoxide Complexes,” no. 22, pp. 5428–5436, 2010.

[40] M. Megamu, S. Kitagawa, and M. Miyazima, “Classification of Solvents Based on Their Coordination Power to Nickel(II) Ion. A New Measure for Solvent Donor Ability,” *Am. Chem. Soc.*, vol. 24, no. 11, pp. 1638–1643, 1985.

[41] B. H. Farnum, J. J. Jou, and G. J. Meyer, “Visible light generation of I–I bonds by Ru-tris(diimine) excited states,” *Proc. Natl. Acad. Sci.*, vol. 108, no. 39, pp. 15628–15633, 2012.

[42] A. Kay, R. Humphry-baker, and M. Gratzel, “Artificial Photosynthesis. 2. Investigations on the Mechanism of Photosensitization of Nanocrystalline TiO2 Solar Cells by Chlorophyll Derivatives,” *Am. Chem. Soc.*, vol. 98, no. 3, pp. 952–959, 1994.